



Computational Science and Engineering  
(International Master's Program)

## Theory of Neuronal Dynamics Group

Max Plack Institute for Brain Research

Master's Thesis

# Heterosynaptic Cooperativity in Pair-based Spike-Timing-Dependent Plasticity (STDP)

Saif Ahmed







Computational Science and Engineering  
(International Master's Program)

## Theory of Neuronal Dynamics Group

Max Plack Institute for Brain Research

Master's Thesis

### Heterosynaptic Cooperativity in Pair-based Spike-Timing-Dependent Plasticity (STDP)

Author: Saif Ahmed  
1<sup>st</sup> examiner: Dr. Tatjana Tchumatchenko  
Thesis advisor: Dr. Andreas Nold  
2<sup>nd</sup> examiner: Prof. Dr. Christina Kuttler  
Submission Date: December 2nd, 2021





I hereby declare that this thesis is entirely the result of my own work except where otherwise indicated. I have only used the resources given in the list of references.

December 2nd, 2021

Saif Ahmed



---

## Acknowledgments

Firstly, I would like to express my gratitude towards Dr. Tatjana Tchumatchenko for allowing me the opportunity to conduct my thesis in her exceptional research group and making me feel part of it. Her trust, encouragement and feedback provided an environment that was supportive and encouraging. It was a pleasure to work along side the incredible people at the lab, many of whom played significant roles towards the completion of this thesis.

I am sincerely grateful to Dr. Andreas Nold for supervising my thesis and his incredible support throughout the process. I was able to unconditionally rely on his feedback, ideas, and direction to make progress in all phases of the thesis including the modeling process, the programming phase as well as the analysis of the simulations. Besides the academic assistance, his ability to motivate and inspire new ideas helped me achieve far more than I could have hoped for.

Thanks to Carlos Wert Carvajal for helping me with the literature research in the first phase of my thesis and for the numerous discussion which unfailingly sparked new ideas and topics for exploration.

Thanks to Pierre Ekelmans for his tremendous support on the existing code base and for his contributions in establishing design principles for the code written for the purposes of this thesis.

Thanks to Prof. Dr. Christina Kuttler for her kindness, support and feedback.



---

## Abstract

Neurons are connected by points of contact, known as synapses. A fundamental property of such a synapse is that the strength of the connection it represents is plastic rather than static. In other words, each synapse has a weight associated with it, which represents the strength of the connection between the presynaptic and postsynaptic neuron, and these weights are subject to change owing to the activity pattern of the two neurons. This dynamic characteristic of synapses is termed plasticity.

Experimentally, we can distinguish between two forms of plasticity: homosynaptic and heterosynaptic plasticity. The two forms differ in their requirement of presynaptic activity during induction. Homosynaptic plasticity is induced in synapses whose presynaptic neurons are directly involved in the plasticity induction process whereas the heterosynaptic case is associated with synapses of presynaptic neurons that are not involved in the induction [5].

In our work, we review existing literature on heterosynaptic plasticity, including experimental evidence as well as the potential roles of this form of plasticity. Furthermore, we use an experimental study to device models of heterosynaptic plasticity to investigate synapse-level implications of this form of plasticity [28].

In order to investigate the effects of our heterosynaptic plasticity mechanism, we use classical, pair-based STDP rules to induce homosynaptic plasticity and augment the STDP to account for the heterosynaptic effects. We use different simulation setups to obtain insights into suitable STDP kernels for heterosynaptically-active neurons as well to analyse spatial patterns that emerge along dendrites due to specific configurations of initial synaptic weights.

We implemented a framework for heterosynaptic plasticity into our existing program for spiking network models to facilitate our simulations. Additionally, an important design goal of the framework was to allow rapid extendibility in terms of new heterosynaptic rules as more experimental or theoretical data on the topic comes to surface.



# Contents

<b>Acknowledgements</b>	vii
<b>Abstract</b>	ix
<b>I. Introduction and Background Theory</b>	1
<b>1. Introduction</b>	3
1.1. Aims and objectives . . . . .	4
1.2. Outline . . . . .	4
<b>2. Background</b>	7
2.1. Neurons, synapses and transmission of information . . . . .	7
2.1.1. Structure of a neuron . . . . .	7
2.1.2. Electrical properties of neurons . . . . .	7
2.1.3. Transmission of information . . . . .	8
2.1.4. The Leaky-Integrate and Fire (LIF) model of a neuron . . . . .	9
2.1.5. Synapses . . . . .	11
2.1.6. Instantaneous synapse model . . . . .	12
2.2. Synaptic plasticity . . . . .	13
2.2.1. Instantaneous synapse model with plasticity . . . . .	13
2.2.2. Categorisation of plasticity . . . . .	13
2.2.3. Homosynaptic long-term plasticity . . . . .	14
2.2.4. Homosynaptic rate-based models . . . . .	17
2.2.5. Homosynaptic STDP Models . . . . .	19
2.3. Heterosynaptic plasticity . . . . .	24
2.3.1. Heterosynaptic plasticity in experiments and computation . . . . .	24
<b>II. Pair-based STDP with heterosynaptic cooperativity</b>	29
<b>3. Pair-based STDP with Heterosynaptic Cooperativity</b>	31
3.1. Modeling heterosynaptic cooperativity in co-activated spines . . . . .	31
3.1.1. Heterosynaptic cooperativity . . . . .	31
3.1.2. Spike-Timing-Dependent Plasticity (STDP) with heterosynaptic cooperativity . . . . .	33

---

## Contents

---

3.1.3. Effects of heterosynaptic cooperativity on the STDP kernel . . . . .	35
3.2. Validation of heterosynaptic STDP with LTP drift . . . . .	36
3.2.1. Setup . . . . .	36
3.2.2. Results and Discussion . . . . .	38
3.3. Spatial effects of Heterosynaptic Cooperativity . . . . .	42
3.3.1. Setup . . . . .	42
3.3.2. Results - Configuration 1 . . . . .	45
3.3.3. Results - Configuration 2 . . . . .	47
3.3.4. Results - Configuration 3 . . . . .	48
3.4. Implementation overview . . . . .	48
3.4.1. Network execution framework . . . . .	49
3.4.2. Heterosynaptic Extensions . . . . .	50
3.4.3. Time-stepping scheme . . . . .	51
3.4.4. Procedures for extensions . . . . .	51
<b>III. Discussion, Limitations and Outlook</b>	<b>53</b>
<b>4. Discussion, Limitations and Outlook</b>	<b>55</b>
4.1. Discussion . . . . .	55
4.2. Assumptions and Limitations . . . . .	56
4.3. Outlook . . . . .	57
<b>Appendix</b>	<b>61</b>
<b>A. Appendix</b>	<b>61</b>
A.1. Synaptic weight normalization . . . . .	61
A.2. Additional results for LTP drift in pair-based STDP . . . . .	61
A.3. Additional simulation results for spatial effect . . . . .	67
A.4. Single neuron synaptic stability . . . . .	70
<b>Bibliography</b>	<b>71</b>

## **Part I.**

# **Introduction and Background Theory**



# 1. Introduction

In experimental studies such those using brain slice cultures, we distinguish two distinct forms of plasticity: homosynaptic and heterosynaptic plasticity. The two differ in their requirement of presynaptic stimulation. In the case of homosynaptic plasticity, the presynaptic neurons of the synapses that change plasticity are directly involved in the plasticity induction process whereas, for synapses involved in heterosynaptic plasticity, no direct involvement of the presynaptic neuron is necessary. This difference in the activity pattern of the presynaptic neuron in the two forms of plasticity is indicative of potentially different roles played by each in the paradigm of learning and memory formation.

Homosynaptic Hebbian-type plasticity has been studied extensively and is widely accepted as the mechanism that enables an organism to differentiate between various recurring stimuli received by the sensory pathways and to establish associations between them. On the other hand, heterosynaptic plasticity is mediated by signaling among neighboring synapses and thus, it has been postulated that this form of plasticity plays a role in maintaining homeostatic balance in neuronal circuits [15, 5] as well as in facilitating synaptic competition [5]. Nonetheless, it is likely that we encounter new forms of intersynapse interactions as further experimental results surface in the coming years which may elicit new functional roles of such intersynapse communication.

One such experimental study, published in 2020, revealed a novel form of heterosynaptic cooperativity in layer 5 pyramidal neurons from juvenile mice [28] (Tazerrart et al. 2020). Broadly, the paper presents a case where multi-synapse stimulation paired with postsynaptic firing can lead to stronger levels of potentiation and weaker depression in comparison to the single-synapse pairing protocols. The results insinuate some form of intersynapse communication that modulates the plasticity behavior of the synapses. In other words, there is a fine-grained transfer of information between the synapses along a dendritic tree which subsequently raises questions regarding the significance of such cross-talk in terms of the behavior of the neuron itself, the implications it has on neighboring neurons to which it is connected and on information encoding, learning and so on.

With the aim of investigating some of these questions, we devised a model of heterosynaptic cooperativity from the data presented in [28]. In our model, each synapse contains a packet of local cooperativity information that is modulated by the input activity on the synapse itself and its proximate neighbors. We followed this up by augmenting a standard Spike-Timing-Dependent Plasticity (STDP) kernel with a heterosynaptic multiplier, such

## *1. Introduction*

---

that the STDP kernel acting on a particular synapse is scaled based on the instantaneous cooperativity at the synapse. The model was then programmed into our simulation engine enabling us to run computational experiments with different setups. We investigated the effect of LTP-drifts in heterosynaptic STDP kernels as well the spatially observable effects synapses exercise on each other by virtue of our model.

In the following chapters, we sequentially introduce, explain and discuss the aforementioned sequence of steps in detail.

### **1.1. Aims and objectives**

Our work is intended to investigate how heterosynaptic cooperativity between synapses influences the plasticity patterns in classical, pair-based Spike-Timing-Dependent Plasticity (STDP) models. It is plausible that intersynapse communication encodes potentially non-trivial information that guides the behavior of synapses along its dendritic tree and in turn, the firing response of the neuron to different external stimuli. We aim to inquire the influence such interchange of information has on the dynamics of a single neuron and eventually, on that of network of neurons.

Additionally, we aim to implement the heterosynaptic cooperativity rule we present in chapter 3 into our simulation engine, using it as a guideline to establish a framework for the computational investigation of a wide range of heterosynaptic cooperation mechanisms. In terms of the implementation of the framework, we aim to obtain high modularity in design in order to enable an arbitrary mix and match of different combinations of homosynaptic plasticity, heterosynaptic cooperativity, and dendritic geometries.

### **1.2. Outline**

The discussion in this report is divided in multiple chapters. The following provides an overview of the different sections.

In chapter 2, we start with a overview of the fundamental concepts and ideas that are essential for the discussions that follow. We briefly review existing literature on neurons, synapses and plasticity from a biological standpoint but more importantly, from a modeling perspective. We introduce Spike-Timing-Dependent Plasticity (STDP), which is special form of temporally-aware plasticity rule, and discuss relevant literature around the topic. The final section of chapter 2 focuses on heterosynaptic plasticity and introduces the experimental results that facilitate the development of the heterosynaptic cooperativity model introduced in chapter 3.

In chapter 3, we introduce our model for heterosynaptic cooperativity and how this works in conjunction with classical, pair-based STDP to determine the evolution of synaptic weights over the course of a simulation. We then present the results of the simulations we use to validate our implementation, namely using the characteristic LTP-drift observed in STDP models.

In chapter 4, we investigate the effect of our heterosynaptic rule on the evolution of synaptic weights when the synapses are grouped into spatial bands with different initial weights, effectively creating boundaries along the dendrite.

In chapter 5, we present an overview of the current implementation along with an outline for its extension for new heterosynaptic rules and dendritic geometries. In addition, we discuss the limitations of the model and present an outlook for the future development of our project.



## 2. Background

### 2.1. Neurons, synapses and transmission of information

In this section, we introduce the basic structure of nerve cells, their defining properties, behaviors, and how these structures and mechanisms enable neurons to transmit information within a network.

#### 2.1.1. Structure of a neuron

Neurons are arguably the most interesting cell types in living organisms. These cells use different electrical and chemical signals to transmit information between different regions of the brain as well as to other parts of the body. Typically, a neuron consists of 4 distinct regions: the cell body, the dendrites, the axon, and the axon terminal. Figure 2.1 provides a simple illustration of a neuron and includes a cell body at the center, a large axon extending out of the cell body side and, numerous branching dendrites along the perimeter of the soma. The cell body or soma contains the genes of the cell and the endoplasmic reticulum. These structures enable the cell body to act as the center for the synthesis of virtually all neuronal proteins. These proteins are necessary, among other things, for the renewal of axon and other nerve termini as well as the assembly of membranous vesicles. Extensions of the cell body generally lead into a single axon or several short dendrites. A typical axon extends for a relatively large distance from the cell body. It carries signals, more precisely action potentials, outwards to other neurons. On the other hand, dendrites branch out in a tree-like manner. Dendrites are specialized to receive chemical signals from other neurons, convert them to electrical impulses and transmit them inward towards the soma [25, 12].

#### 2.1.2. Electrical properties of neurons

The critical electrical properties that a neuron exhibits are a consequence of the neuronal membrane, which is made up of two layers of lipid molecules, forming a lipid bilayer. These lipids contain hydrophobic heads which prevent unwanted diffusion of ions across the membrane since the ions are surrounded by clouds of water molecules. On the other hand, the membrane contains pore-forming membrane proteins, known as leakage channels, which selectively allow ions to pass through the membrane. Two of the most commonly encountered leakage channels are the  $\text{Na}^+$  and  $\text{K}^+$  channels. As a consequence of these structural features, the neuronal membrane has different permeabilities for different particles (ions or proteins) and thus the intracellular and extracellular concentrations of

## 2. Background

---

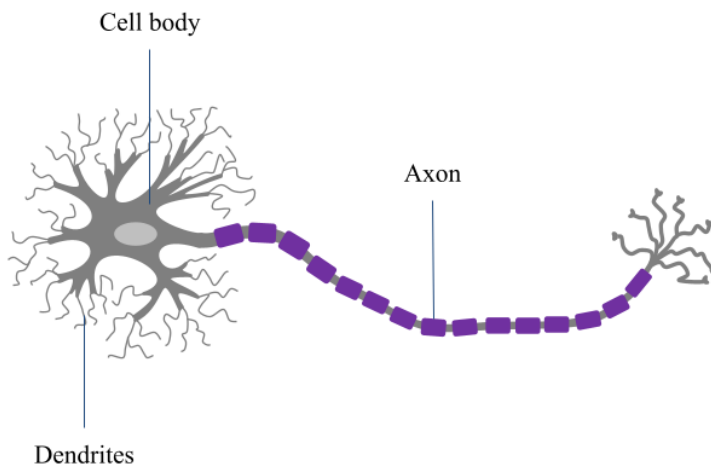


Figure 2.1.: Illustration of a typical neuron by Danylo Batulin.

these particles are unequal. Moreover, the number of leakage channels for cations does not correspond equally to the number for anions. This creates an unequal distribution of charge across the membrane and when the chemical gradient across the membrane equals the electrical gradient across it, the system is said to be in equilibrium. In this state of equilibrium, the potential across the membrane is known as the resting potential of the neuron. The resting potential of excitable neurons generally lies between  $-60$  to  $-95$  millivolts [25].

Besides the leakage channels, the membrane of a neuron contains other ion channels which are gated. The three main types of gated ion channels are ligand-gated, voltage-gated, and mechanically-gated. The channels are in either of three states, open, closed, or inactive, depending on the factors that control them. For example, a ligand-gated channel is open when a specific particle, known as a ligand, binds to the channel whereas a voltage-gated channel opens in response to changes in the membrane potential. The opening of such channels allows changes in the permeability of the membrane to specific ions, enabling depolarisation or hyperpolarisation of the neuron. An extreme example of this is an action potential (AP), which is a sudden, rapid change in the membrane potential, illustrated and described in Figure 2.2 [25].

### 2.1.3. Transmission of information

When a neuron undergoes an AP sequence, the neuron is said to have spiked and this spike in membrane potential propagates along its axon. At the terminal parts of the axon, specialized chemical machinery allows the electrical spike to be converted into a chemical signalling cascade that releases transmitters into the surrounding cavity, known as a synaptic cleft. Typically, this cavity contains dendritic extensions, or spines, of one or more neighboring neurons which in turn are able to chemically detect changes in the synaptic

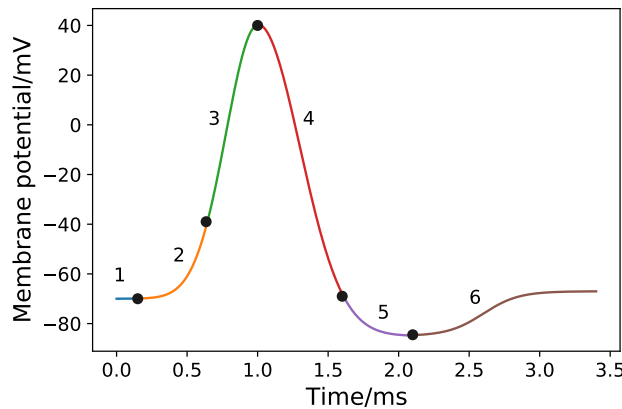


Figure 2.2.: Membrane potential over time during a typical action potential sequence.

1. A neuron is initially in equilibrium with the membrane potential at the resting value.
2. Ligand-gated sodium channels on the membrane open due to binding of neurotransmitter. This causes an influx of sodium causing a depolarisation of the neuron.
3. As the neuron starts depolarising, it reaches a certain threshold. Once the membrane potential exceeds this threshold, it triggers the opening of voltage-gated sodium channels. This, further amplifies the influx of sodium ions into the neuron. The membrane potential spikes.
4. After a slight delay, voltage-gated potassium channels open, causing an outflux of potassium ions from the neuron. This outflux opposes the influx of sodium in terms of the ion flow and starts a repolarisation.
5. As the repolarisation proceeds, the voltage-gated sodium channels close, and the neuron repolarises to below the resting potential, a phenomenon known as afterhyperpolarization.
6. Once the voltage-gated potassium channels close, the neuron gradually returns to its original resting potential.

cleft and transmit the spiking information to the cell body of these neighboring neurons as an electrical impulse. The axonal terminal of the first neuron, the synaptic cleft, and the dendritic spine of the second neuron together form a so-called synapse, which is further elaborated in section 2.1.5. A synapse, thus, serves as the structural unit for the transmission of spiking information between neurons.

#### 2.1.4. The Leaky-Integrate and Fire (LIF) model of a neuron

Computational models of a single neuron can be quite complex. Since the dynamics of a neuron depend on the interplay of different non-linear ionic conductances, aiming to capture these can result in models with multiple coupled ODEs. Therefore, depending on the computational goals of a particular simulation, some models might be more suitable than

## 2. Background

---

others.

The simplest class of neuron models are the integrate-and-fire models. The basis of such models is the fact that all action potentials of the same neuron are roughly similar in their dynamics. This hints at the idea that information is not transmitted in the shape of the action potential but rather on the existence of a spike, essentially reducing the neuron to an event-based system where a spike or action potential is regarded as an event [9]. One such model, the Leaky-Integrate and Fire (LIF) neuron is discussed in detail in this section since it is the neuron model of choice for our simulations in later chapters.

The LIF neuron model is derived from the idea that the membrane of a neuron can essentially be viewed as an RC circuit. As mentioned previously, the charges across the membrane are unequally distributed. This, together with the insulating characteristics of the membrane mean that it functions as a capacitor. Moreover, due to the flow of ions through the passive ion channels on the membrane, it acts as a resistor as well. This is illustrated in Figure 2.3.

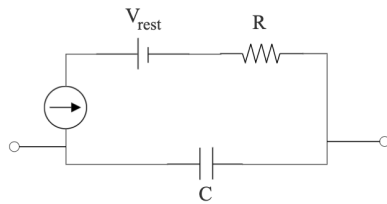


Figure 2.3.: RC-circuit representing the neuronal cell membrane. The potential difference across the two end terminals represents the membrane potential.

This means that the current through the cell membrane at any time  $t$ , can be represented by two components, a resistive current,  $I_R$  and a capacitive current  $I_C$ :

$$I(t) = I_R(t) + I_C(t) \quad (2.1)$$

Using Ohm's law and the definition of capacitance, equation 2.1 can be rewritten as follows [9]:

$$I(t) = \frac{V(t) - V_{rest}}{R} + C \frac{dV}{dt} \quad (2.2)$$

where:

- $V(t)$  represents the membrane potential at time  $t$
- $V_{rest}$  represents the resting potential

Finally, by introducing the time constant  $\tau_m = RC$  and reordering the terms in 2.2, we get the differential equation in 2.3:

$$\tau_m \frac{dV}{dt} = -[V(t) - V_{rest}] + RI(t) \quad (2.3)$$

Besides the above equation, two additional parameters determine the behavior of the LIF neuron. The first is a voltage threshold  $V_\theta$  which determines the threshold above which the neuron elicits an AP. Once  $V_\theta$  is reached, the neuron records a spike and the membrane potential is reset to  $V_{rest}$ . The second is the refractory time,  $\tau_{ref}$ , which determines the time after a spike during which a neuron is not capable of producing additional spikes. This can be achieved either by keeping the potential fixed at the resting potential, by adding a conductance that induces a strong transient hyperpolarisation directly after the spike, or by allowing the resting value membrane potential to change. In our implementation, we opt for the first option [9].

Clearly, the LIF model is a highly simplified model which ignores ion channels and their respective conductances. Moreover, the shape of the AP is disregarded and represents a loss in information. Therefore, we cannot expect it to explain the intricate biochemistry and the biophysics of the neuron and its spiking mechanism. However, it has proven to be quite accurate when analysing spiking behavior of neurons and works well as a event-based system [9]. Since the simulations we present later are concerned with spiking behavior rather than detailed biophysical interactions, the model serves well for our work.

### 2.1.5. Synapses

Synapses are the specialized structures that allow neurons to communicate with each other. As mentioned previously, a spiking neuron transmits its action potential through its axon and into the dendrites of other neurons. The point of contact between an axonal terminal of a presynaptic neuron and the dendritic spine of a postsynaptic neuron is called a synapse. On average, a neuron forms several thousand synaptic connections and receives a similar number. In chemical synapses, the process that mediates transmission of electrical signals between neurons at the synapse is a complex multi-step process in which calcium ions ( $Ca^{2+}$ ) play a critical role [25].

The diffusion of neurotransmitters through the synaptic cleft mediates the transmission of signals across the synapse. The following steps provide an overview of a typical ionotropic synaptic transmission:

1. The arrival of an action potential at the terminal end of the axon of the presynaptic neuron causes the opening of voltage-gated  $Ca^{2+}$  channels in the region.
2. The influx of calcium in the intracellular region of the presynaptic neuron causes synaptic vesicles, which are organelles containing neurotransmitters, to fuse to the cell membrane and release neurotransmitters into the synaptic cleft.

## 2. Background

---

3. The neurotransmitters in the cleft then bind to the ligand-gated channels on the postsynaptic side of the synapse which may trigger an action potential sequence on the postsynaptic neuron.

The above sequence of steps describes the workings of an ionotropic, excitatory synapse, wherein the presynaptic neuron facilitates an action potential generation on the postsynaptic neuron. However, another important class of synapses are inhibitory synapses which act in the opposite way, where the transmission of an AP from the presynaptic neuron acts to inhibit an AP on the postsynaptic neuron. This difference in such synaptic functionality depends on the type neurotransmitter that is released into the synaptic cleft [25].

### 2.1.6. Instantaneous synapse model

The modeling of a synapse involves the choice by which spikes in postsynaptic neurons are integrated into a current component for the presynaptic neuron. In equation 2.3, for example, this would be the term  $I(t)$ . Generally, the integration of postsynaptic inputs involves a conductance term for each synaptic input which is multiplied to the presynaptic current. In our simulations, we use an instantaneous synapse to integrate presynaptic inputs into the postsynaptic neuron. It is simple but one of the most fundamental models and is widely used in literature to model synapses. An instantaneous synapse is characterised by a conductance or coupling term that encodes the amount of current that passes through the synapse when the presynaptic neuron fires. In the simplified case where we consider only the spiking behavior of the presynaptic neuron and the coupling strength between two neurons remains constant, synaptic transmission through an instantaneous synapse can be represented by the equation 2.4 [36].

$$I(t) = J \sum_k \delta(t - t^{(k)}) \quad (2.4)$$

where:

- $J$  represents the coupling strength of the synapse
- $t^{(k)}$  represents the arrival time of the  $k^{th}$  presynaptic spike

If we extend the equation (2.4) such that a postsynaptic neuron receives inputs from multiple presynaptic neurons, the equation involves an additional summation term as shown in equation 2.5.

$$I(t) = \sum_i J_i \sum_k \delta(t - t_i^{(k)}) \quad (2.5)$$

where:

- $J_i$  represents the coupling strength of the synapse involving presynaptic neuron  $i$

- $t_i^{(k)}$  represents the arrival time of the  $k^{th}$  presynaptic spike from the  $i^{th}$  presynaptic neuron

## 2.2. Synaptic plasticity

In the previous section, we introduced synapses as static entities wherein the coupling between two neurons is constant. However, the coupling strength or synaptic efficacy is in fact dynamic and is subject to change owing to the firing patterns of the two neurons in question. Although this idea was rejected for some time after it was first introduced, extensive research over the past century has confirmed that indeed the neural pathways of the brain are not rigid but rather plastic, hence the term plasticity was coined [3]. Moreover, plasticity encompasses a bidirectional change in synaptic efficacy meaning that synapses are capable of strengthening and weakening based on the activity patterns of the presynaptic or postsynaptic neurons or both. The strengthening of a synapse is referred to as potentiation whereas depression refers to the weakening of a synapse.

### 2.2.1. Instantaneous synapse model with plasticity

The instantaneous synapse model introduced in equation 2.4 requires a slight modification in order to incorporate plasticity. The requirement being that the conductance of a particular synapse changes from being a constant to a variable that can be changed based on certain rules of plasticity. In order to vary the conductance or the synaptic efficacy of a synapse, we introduce an additional factor,  $w$ , as shown in 2.6. Although this can be achieved by allowing the conductance term  $J$  to be variable, we opt for the extra factor in order to maintain consistency with the implementation. Generally, an ODE is used to determine the dynamics of  $w$  based on the firing patterns or more generally, the activity patterns of the presynaptic and postsynaptic neurons.

$$I(t) = wJ \sum_k \delta(t - t^{(k)}) \quad (2.6)$$

where:

- $w$  represents the weight or efficacy of the synapse

### 2.2.2. Categorisation of plasticity

Synapses exhibit different forms of plasticity with the differentiating characteristics being the strengthening or weakening of synapses, the timescales over which the plasticity lasts as well as the direct or indirect involvement of the presynaptic neuron of the synapse in the plasticity-inducing mechanism.

## 2. Background

---

**Direction of plastic change.** A synapse may undergo two types of changes in terms of its strength. A strengthening of a synaptic connection is referred to as potentiation, whereas a weakening is termed depression. In our simulations, the synaptic efficacy,  $w$ , is allowed to vary between  $w_{min}$  (=0) and  $w_{max}$  (=2). At  $w_{min}$ , a synapse is depressed into silence and plays no role in the dendritic integration at the postsynaptic neuron. Conversely, at  $w_{max}$  a synapse is most conductive. Experimental evidence suggests that a rise in intracellular  $Ca^{2+}$  concentration plays a critical role in the induction of synaptic plasticity [15]. However, whether the direction of the plastic change can be fully explained by the  $Ca^{2+}$  concentration alone is not fully understood. For example, experiments conducted on the spines of the basal dendrites of layer 2/3 pyramidal neurons showed that the  $Ca^{2+}$  concentration determined the magnitude of the plastic change, however, was uncorrelated to the direction of the change [19]. On the other hand, tetanic stimulation of spines in hippocampal CA1 pyramidal cells elicited that concentrations of  $Ca^{2+}$  above a certain threshold triggered NMDAR-dependent (section 2.2.3) long-term potentiation (LTP), whereas a moderate concentration elicited long-term depression (LTD) [1].

**Timescales.** The timescales over which a particular expression of plasticity lasts depend on the underlying biological processes that induce it. Generally, plasticity is categorized into two groups based on their timescales: short-term plasticity and long-term plasticity. Short-term plasticity lasts in the order of milliseconds to several minutes. On the other hand, long-term plasticity lasts for minutes and up to hours [1].

**Homosynaptic vs Heterosynaptic.** Lastly, plasticity can be classified as either homosynaptic or heterosynaptic. Homosynaptic plasticity is the type of plasticity that preserves input-specificity, meaning that only synapses whose presynaptic neurons are directly stimulated or activated in the plasticity-inducing process change efficacy. On the other hand, heterosynaptic plasticity is exhibited by synapses whose presynaptic neurons have no direct involvement in the induction or in other words, the input-specificity of the homosynaptic case is not preserved. For example, consider a hypothetical neuron with two synapses, A and B. Synapse A is stimulated with a high-frequency tetanic input to elicit potentiation. Without the existence of heterosynaptic plasticity, only synapse A would potentiate and the efficacy of synapse B would remain unchanged. However, if there exists some form of heterosynaptic plasticity, synapse B may undergo a certain degree of potentiation or depression.

### 2.2.3. Homosynaptic long-term plasticity

In the remaining chapters we develop a rule for long-term plasticity. Therefore, we briefly turn our discussion towards the experimental evidence of long-term plasticity and the biological processes that are involved.

### Discovery of long-term plasticity.

The first half of the twentieth century marked the publication of multiple experimental demonstrations of short-term plasticity as well as post-tetanic potentiation. These results sparked widespread interest in the idea of plasticity and several consequent theories and experimental studies lead to the discovery of long-term plasticity.

Donald Hebb, in 1949, postulated the idea that when a neuron, A, repeatedly and persistently contributes to the firing of another neuron, B, the connection between the two neurons undergoes certain metabolic changes that increase the strength of their connection. This, in turn, allows neurons to form associations with other neurons, establishing the foundations of learning and memory [14]. The introduction of Hebbian plasticity was a vital breakthrough for future developments and the discovery of plasticity rules, as it served as the premise for numerous experimental, research projects.

About two decades after Hebb's publication, a number of papers presented evidence of LTP in the rabbit hippocampus [22, 21]. It was shown that high-frequency tetanic stimulation of the perforant pathway to the dentate gyrus resulted in potentiation that lasted for much longer periods than those observed in the case of short-term plasticity. Future experiments resulted in the discovery of properties of LTP that established it as a Hebbian process. The most important ones include [20]:

- **Cooperativity:** A weak input characterized by the simultaneous tetanization of only a few synapses was incapable of inducing LTP. However, increasing the number of tetanized synapses reliably induced LTP, indicating some form of homosynaptic synaptic cooperation.
- **Input-specificity:** When LTP was induced, only the tetanized pathways exhibit synaptic modification.
- **Associativity:** A weak synaptic input incapable of inducing LTP on its own , exhibited LTP when tetanized simultaneously with a strong input on another synapse.

Following the discovery of LTP, evidence of homosynaptic LTD followed shortly. In experiments done on the rat hippocampus, it was shown that when the high-frequency tetanization used to induce LTP was replaced with a sufficiently low-frequency stimulus, the activated pathways demonstrated LTD [11, 32]. This prompted an extension to Hebb's postulate to incorporate LTD. Additionally, further observations indicated that high-frequency tetanization of synapses as an LTP-induction mechanism could be substituted by coupling postsynaptic depolarization with presynaptic stimulation [20]. This essentially paved the way for the discovery of spike-timing-dependent plasticity (STDP) [4].

---

## 2. Background

---

### **Discovery of homosynaptic Spike-Timing-Dependent Plasticity (STDP).**

STDP is a form of long-term plasticity where the change in synaptic efficacy of a connection depends precisely on the temporal relationship between the presynaptic input and the postsynaptic spike. The first publications that introduced this phenomenon appeared between 1997 and 1998 [29]. Experiments were conducted by pairing presynaptic inputs to postsynaptic APs and it was observed that the precise temporal order of the two signals determined whether presynaptic inputs were subsequently amplified or depressed. When a presynaptic input that causes a postsynaptic EPSP preceded the postsynaptic AP, the synaptic connection experienced potentiation whereas the reverse sequence resulted in depression [4, 35, 30]. Investigation of the window over which coincidences of the two signals were significant indicated that the APs and EPSPs must coincide within 100 ms in order to induce any changes in synaptic efficacy [13]. Additionally, experiments conducted with NMDAR blockers in [13] caused a loss of plastic changes which suggested that the back-propagation of APs into the dendrite cause an influx of  $Ca^{2+}$  which activates the NMDARs and triggers the synaptic modification process.

In terms of computational models, STDP has been widely adopted as a primary learning rule. However, the relative importance of STDP versus local associative or correlation-dependent plasticity in the brain remains to be understood [8].

### **Biological processes involved in long-term plasticity**

In order to introduce the biological processes that mediate one of the most common types of long-term plasticity, NMDAR-dependent plasticity, we must discuss two important receptor families that are involved in the process. The first class of receptors is the AMPARs or  $\alpha$ -amino-3-hydroxy-5-methyl-4-isoxazolepropionic acid and these receptors are activated by the neurotransmitter glutamate. The channels of AMPARs are permeable to both  $Na^+$  and  $K^+$  ions and it is the inward current through these receptors that is the primary source of excitatory synaptic responses that lead to excitatory postsynaptic synaptic potentials (EPSPs). The second is the NMDARs or N-methyl-D-aspartate (NMDA) receptors. These receptors are ligand-gated (ionotropic) cation channels that are activated, once again, by the neurotransmitter glutamate. At negative membrane potentials, NMDARs are blocked by extracellular magnesium. Therefore, these receptors are not involved in the postsynaptic responses of a neuron. However, upon sufficient depolarization of the postsynaptic neuron, the magnesium dissociates from the channels and  $Ca^{2+}$ , as well as  $Na^+$  ions can flow through and into the intracellular cavity [1].

NMDAR-dependent increase in calcium concentrations at the site of synapse on the dendrite can lead to LTP given that the calcium influx is large enough. Upon such an influx, intracellular signaling cascades involving protein kinases such as CaMKII, are triggered. These signaling cascades have a two-fold effect. Firstly, they increase the synaptic conduc-

tance of existing AMPARs, and secondly, they promote the incorporation of more AMPARs at the postsynaptic dendritic site. The resultant effects in an increase in overall synaptic efficacy or in other words, long-term potentiation [1, 26]. Similar to LTP, LTD is also induced by an increase in NMDAR-dependent increase in calcium concentrations. The difference is that for LTD induction, a moderate rather than a high increase in calcium concentrations are required. When the calcium concentrations are indeed moderate, protein phosphatases such as calcineurin are activated instead of kinases as in the case of LTP. Consequently, these phosphatases lead to the disassociation of AMPARs from the postsynaptic density. The synaptic efficacy decreases and we observe long-term depression [1, 26].

The biological process for NMDAR-dependent STDP works by the same mechanism. A coincidence of a presynaptic input with a postsynaptic AP in the pre-post order results in large calcium influx and hence LTP. On the other hand, a coincidence in the post-pre temporal order results in a moderate influx of calcium and as described above, results in LTD [13]. Nonetheless, mechanistic questions such as how neuromodulators regulate STDP and how LTD coincidence detection is performed, remain to be answered [8].

#### 2.2.4. Homosynaptic rate-based models

The experimental discovery of long-term plasticity was accompanied by a bulk of theoretical works which presented mathematical models of the phenomenon. Owing to tetanic induction protocols that uncovered plasticity, the first plasticity models were characterized by the idea that postsynaptic activity is determined by presynaptic activity.

The basic formulation of rate-based models is defined by equation 2.7.

$$\tau_r \frac{dv}{dt} = -v + F(\vec{w} \cdot \vec{u}) \quad (2.7)$$

where:

- $\tau_r$  represents the time constant that determines the firing rate dynamics
- $v$  represents the postsynaptic firing rate
- $\vec{u}$  represents each of the presynaptic firing rates as a vector
- $\vec{w}$  represents the weight of each of the synapses of the postsynaptic neuron as a vector
- $F$  represents the steady-state firing rate as a function of somatic input current or a so called activation function

The changes in postsynaptic activity are directly derived from the combination of all presynaptic activity. Individual models of such a rate-based model family differ in the mechanism by which these weights are updated [23].

## 2. Background

---

### Homosynaptic Hebb's rule

To capture the basis of Hebb's postulate in terms of the update of synaptic weights, one could use equation 2.8 with the right-hand side of the equation being interpreted as the probability that presynaptic and postsynaptic activity coincide [23].

$$\tau_w \frac{d\vec{w}}{dt} = v\vec{u} \quad (2.8)$$

where:

- $\tau_w$  represents the decay constant for synaptic weights

The problem with the simple rule above is that it cannot capture LTD. Since the firing rates will  $u$  and  $v$  are non-negative, the model allows only positive changes in synaptic efficacy, or more precisely LTP. Moreover, such a model is unstable and the synaptic weights tend to saturate since Hebb's postulate is inherently a positive feedback process. To elaborate, in Hebbian plasticity, synapses that effectively contribute to postsynaptic firing are strengthened which further enhances their effectiveness. As a result, individual synapses tend to saturate towards the maximal weight over the course of a simulation.

### Homosynaptic co-variance rule

In order to account for LTD, equation 2.8 can be modified to 2.10 [23]. In this so-called co-variance rule, a threshold for postsynaptic activity,  $\theta_v$ , is incorporated with the idea that when the postsynaptic activity exceeds this threshold the change in synaptic efficacy upon presynaptic and postsynaptic coincidence (pre-post coincidence) is reversed from being positive to being negative. Therefore, at times of high postsynaptic activity, pre-post coincidences result in LTD whereas at times of low postsynaptic activity the resultant change is LTP.

$$\tau_w \frac{d\vec{w}}{dt} = (v - \theta_v)\vec{u} \quad (2.9)$$

where:

- $\theta_v$  represents postsynaptic activity threshold above which LTP switches to LTD

Nonetheless, the positive feedback characteristic described for the simple Hebb's rule is retained and consequently, the co-variance rule does not provide stable models.

### Homosynaptic BCM rule

To overcome the caveats of the previously introduced rate-based models, the BCM rule was introduced in 1982. This model incorporates a sliding threshold,  $\theta_v$ , instead of a fixed one. In this case,  $\theta_v$  is coupled with the postsynaptic activity and increases as the postsynaptic activity grows. In order for the model to be stable, the growth of  $\theta_v$  must be faster

than the increase in the postsynaptic rate  $v$ . This ensures that when a certain group of synapses becomes strongly potentiated, the possibility of other synapses getting potentiated becomes less likely, essentially enabling synaptic competition [23]. An example of the dynamics of  $\theta_v$  as a function of the postsynaptic rate is presented in .

$$\tau_\theta \frac{d\theta_v}{dt} = v^2 - \theta_v \quad (2.10)$$

where  $\tau_\theta$  represents the decay constant for sliding threshold

### 2.2.5. Homosynaptic STDP Models

Rate-based models, particularly the BCM rule, paved the way for widespread theoretical and experimental research on synaptic plasticity. Nonetheless, since the discovery of STDP, it was clear that such models fail to incorporate any of the interesting temporal dependence between presynaptic and postsynaptic spikes. Therefore, in this section, we present the Graupner STDP as well as the pair-based STDP model, the latter of which is used in our models in later sections.

#### Homosynaptic calcium-based plasticity model (Graupner model)

The Graupner model was derived from the idea that a synapse undergoes potentiation or depression depending on the influx of  $Ca^{2+}$  concentration. A sufficiently high intracellular  $Ca^{2+}$  concentration results in potentiation, whereas a moderate influx results in depression. The idea is mathematically realized by equation 2.11 [10].

$$\tau_w \frac{dw}{dt} = -w(1-w)(w_* - w) + \gamma_P(1-w)\Theta[c(t) - \theta_P] - \gamma_D w\Theta[c(t) - \theta_D] + Noise(t) \quad (2.11)$$

where:

- $\tau_w$  represents the decay constant for synaptic weights
- $w$  represents the synaptic weight of a single synapse
- $w_* = 0.5$  represents the boundary of the basins of attraction of two possible stable states ( $w = 0$  and  $w = 1$ )
- $c(t)$  represents the calcium concentration at time t
- $\theta_P$  represents the calcium threshold above which synapse potentiates
- $\theta_D$  represents the calcium threshold above which synapse depresses
- $\gamma_P$  represents the magnitude of potentiation when the  $\theta_P$  is exceeded

## 2. Background

---

- $\gamma_D$  represents the magnitude of depression when the  $\theta_D$  is exceeded
- $Noise(t)$  represents a noise term added to the model
- $\Theta$  represents the heavy-side function

As expressed in equation 2.11, calcium concentrations determine the direction of synaptic change. Each synapse keeps track of local calcium concentrations where calcium transients are elicited by both presynaptic and postsynaptic spiking. Postsynaptic firing results in larger rises in calcium concentrations in comparison to presynaptic input spikes [10]. The model produces two different stable points for the weight of a synapse,  $w_{min} = 0$  and  $w_{max} = 1$ . At  $w_{min}$  a synapse is silent and loses all influence on the postsynaptic firing and at  $w_{max}$  a synapse is maximally potentiated. Although the Graupner model is not derived directly from the basic idea of STDP, it was shown that when the following conditions were imposed, the model can reproduce classical STDP:

- $\theta_P > \theta_D$
- $C_{post} > \theta_P$ , where  $C_{post}$  the calcium transient when there is postsynaptic firing
- $C_{pre} > \theta_P$ , where  $C_{pre}$  the calcium transient when there is presynaptic firing

### Pair-based STDP

STDP relies on temporal information of presynaptic and postsynaptic spikes to induce changes in synaptic efficacy. A pre-post event sequence results in potentiation whereas a post-pre event causes depression. Such models which rely on pair-wise interactions between pre and post spikes are referred to as pair-based STDP models. [9]

With this idea as the foundation, we introduce a general form of the pair-based STDP model for a synapse,  $i$ , of a neuron with multiple synapses in equation 2.12.

$$\frac{dw_i}{dt} = A_{LTP} \sum_{\forall j} \delta(t - t_{post}^{(j)}) K(t_{post}^{(j)} - t_{i,pre}^{(last)}) + A_{LTD} \sum_{\forall j} \delta(t - t_{i,pre}^{(j)}) K(t_{i,pre}^{(j)} - t_{post}^{(last)}) \quad (2.12)$$

where:

- $w_i(t)$  represents the synaptic efficacy for synapse  $i$
- $A_{LTP}$  represents the maximal potentiation that a synapse can undergo under one pair-based event

- $A_{LTD}$  represents the maximal depression that a synapse can undergo under one pair-based event
- $K_{LTP}$  represents the kernel used for potentiation/depression (kernel functions map pre-post (post-pre) sequences to plasticity changes)
- $t_{post}^{(j)}$  represents the arrival time of the j-th postsynaptic spike
- $t_{i,pre}^{(last)}$  represents the arrival time of the temporally nearest presynaptic spike at synapse i at time t with  $t_{i,pre}^{(last)} < t$
- $t_{i,pre}^{(j)}$  represents the arrival time of the j-th presynaptic spike at spine i
- $t_{post}^{(last)}$  represents the arrival time of the temporally nearest postsynaptic spike at time t with  $t_{post}^{(last)} < t$

The first term on the right-hand side of 2.12 captures LTP behavior. The delta function in the summation term encodes the mechanism that a check for synaptic potentiation is done on every postsynaptic spike of the neuron. The magnitude of the potentiation is determined by the LTP kernel. Similarly, the second term is associated with LTD. In this case, a check for synaptic depression is done on every presynaptic spike at synapse i of the neuron. One important aspect of the model presented above is that the presynaptic and postsynaptic interactions are of the so-called nearest-neighbor interaction. This means each presynaptic or postsynaptic spike interacts with the nearest temporally trailing postsynaptic and presynaptic spike respectively. An alternative would be to consider all trailing spikes in an all-to-all manner [29].

### STDP Kernels

The kernel functions introduced in the previous section essentially determine the difference in timing between a pre (post) and post (pre) spike at which LTP (LTD) is maximal.

**The E-kernel.** The first kernel we introduce is the E-kernel. This is the most common kernel used in literature for STDP models. It is characterized by decaying exponential functions as shown in equation 2.13. The kernel is graphically in figure 2.4 [9].

$$K_e(\Delta t) = \begin{cases} \exp\left(-\frac{\Delta t}{\tau_{LTP}}\right) & \text{if } \Delta t > 0, \\ -\exp\left(\frac{\Delta t}{\tau_{LTD}}\right) & \text{if } \Delta t < 0, \\ 0 & \text{Otherwise} \end{cases} \quad (2.13)$$

where:

## 2. Background

---

- $\Delta t$  represents the timing difference between a postsynaptic and a presynaptic spike. Positive values of  $\Delta t$  represent events where a presynaptic spike precedes a postsynaptic spike, negative values represent events where a postsynaptic spike precedes a presynaptic one
- $\tau_{LTP}$  represents the LTP decay constant
- $\tau_{LTD}$  represents the LTD decay constant

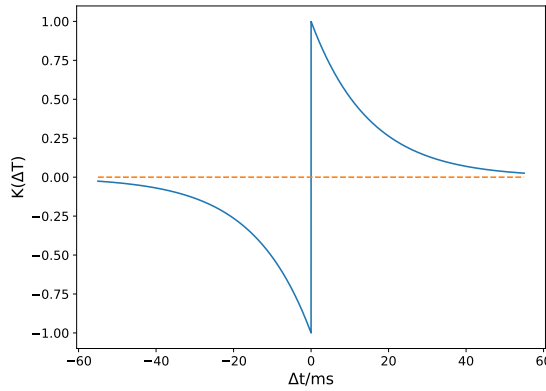


Figure 2.4.: Graphical representation of the E-kernel. The kernel prefers pre and post spikes to be temporally nearby in order to maximise plasticity. As the timing between a pre (post) and a post (pre) spike increases, the LTP (LTD) decreases exponentially.

**The G-kernel.** The second kernel we use in our work is derived from the experimental results in [28]. In this case, the kernel prefers a specific  $\Delta t$  that produces maximal LTP/LTD, one which is not necessarily the smallest possible absolute value. The behavior is modeled as a two-sided Gaussian function as shown in equation 2.14. The kernel is graphically in figure 2.5.

$$K_g(\Delta t) = \begin{cases} \exp\left(-\frac{(\mu_{LTP}-\Delta t)^2}{2\sigma_{LTP}^2}\right) & \text{if } \Delta t > 0, \\ -\exp\left(-\frac{(\mu_{LTD}-\Delta t)^2}{2\sigma_{LTD}^2}\right) & \text{if } \Delta t < 0, \\ 0 & \text{Otherwise} \end{cases} \quad (2.14)$$

where:

- $\Delta t$  represents the timing difference between a postsynaptic and a presynaptic spike. Positive values of  $\Delta t$  represent events where a presynaptic spike precedes a postsynaptic spike, negative values represent events where a postsynaptic spike precedes a presynaptic one

- $\mu_{LTP}$  represents the position of the center of the LTP window
- $\mu_{LTD}$  represents the position of the center of the LTD window
- $\sigma_{LTP}$  represents the width of the LTP window
- $\sigma_{LTD}$  represents the width of the LTD window

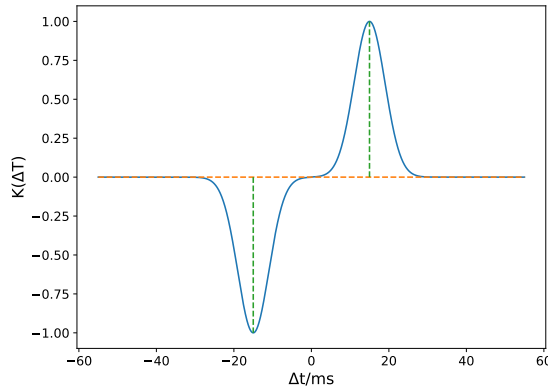


Figure 2.5.: Graphical representation of the G-kernel. The kernel has specific preferential values ( $\mu_{LTP}$  and  $\mu_{LTD}$ ) of  $\Delta t$  marked by the dashed green lines at which LTP and LTD are maximised.

It is important to note that the kernel illustrations above depict symmetrical windows for LTP and LTD. In such a configuration, a neuron with a given number of Poisson inputs, capable of evoking postsynaptic spikes, would result in the mean synaptic weights drifting towards the maximal synaptic weight. Possible treatment of this issue would be to have a more pronounced LTD window (this issue is revisited in the next chapter when our implementation of STDP is validated).

### Limitations of pair-based STDP

Several caveats of a simple pair-based STDP model have been published in literature. The most important are noted below.

**Pair-based models fail to capture frequency dependence of long-term plasticity.** Experiments for long-term potentiation using tetanic stimulation show that high-frequency simulations of synaptic inputs result in potentiation of the synapses whereas low-frequency simulations result in depression. However, a pair-based STDP model is unable to capture such frequency-dependent plasticity. For example, for a given number of repetitions of

## 2. Background

---

pre-post pairings, pair-based models would result in the same amount of LTP/LTD irrespective of the stimulation frequency [24].

**Pair-based models fail to capture triplet and quadruplet experiments.** The idea of pair-based models stemmed from the early experiments of STDP which used pairs of presynaptic and postsynaptic spikes to determine changes in synaptic efficacy. However, this does not imply that pairs of spikes are the elementary blocks of STDP. Therefore, further experiments were conducted with triplets and quadruplets of spikes and it was shown that a pair-based model was unable to account for the observations in these experiments [24]. For example, experiments in [34] showed that triplet pairings of the sequence pre-post-pre (presynaptic spike followed by a postsynaptic spike and finally another presynaptic spike) and post-pre-post resulted in different plasticity behavior than that predicted by a pair-based model. In a pair-based model, a pre-post-pre sequence would elicit potentiation, followed by depression. Similarly, a post-pre-post sequence would evoke depression and potentiation. Although the order of the potentiation and depression are reversed, pair-based STDP would predict that the net change in plasticity would be the same for both sequences. However, in [34] it was shown that while pre-post-pre triplets did not induce any significant plasticity change, post-pre-post triplets resulted in a marked potentiation of the synapse. Besides this example, other plasticity behaviors under triplet and quadruplet pairings cannot be captured using pair-based STDP rules.

Nonetheless, since our simulations are directed at exploring heterosynaptic effects rather than direct comparisons of differing frequencies of induction or patterns of induction, we use the relatively simple, pair-based model for our work.

### 2.3. Heterosynaptic plasticity

In this section, we introduce experimental evidence of different forms of heterosynaptic plasticity and several published models that capture them. In addition, we briefly discuss the roles and functions of these different forms.

#### 2.3.1. Heterosynaptic plasticity in experiments and computation

The first experimental evidence of heterosynaptic plasticity was observed during the discovery of LTD, discussed in 2.2.3. The induction of LTP at the input at the apical dendrite of CA1 pyramidal neurons was accompanied by LTD at the inputs at the basal dendrite [11, 32]. This suggested that input specificity effectively broke down at short distances and neighboring synapses were heterosynaptically modified. Heterosynaptic LTP was discovered in pairing experiments for inputs of a CA1 neuron in the hippocampus. It was observed that LTP induction of the paired input resulted in weaker LTP in the synapses formed by nearby fibers [31, 6, 7].

### Mexican-hat shaped heterosynaptic plasticity

Further studies followed that revealed more detailed heterosynaptic effects. In particular, it was demonstrated that heterosynaptic changes experienced by neighboring synapses are dependent on their relative distance from the point of induction [27] in structures that are regularly organized, such as the hippocampus or amygdala. Induction of LTP on a set of synapses in such regions produced a Mexican hat-shaped response where nearby synapses experienced weaker LTP, followed by LTD at larger distances before the distance becomes too large to cause any heterosynaptic change. A complimentary response was observed for LTD where nearby induced synapses experienced weaker LTD, with LTP for synapses that are further away and eventually no change. Figure 2.6 represents two scenarios of distribution of plasticity after a synapse undergoes LTP (left) and LTD (right).

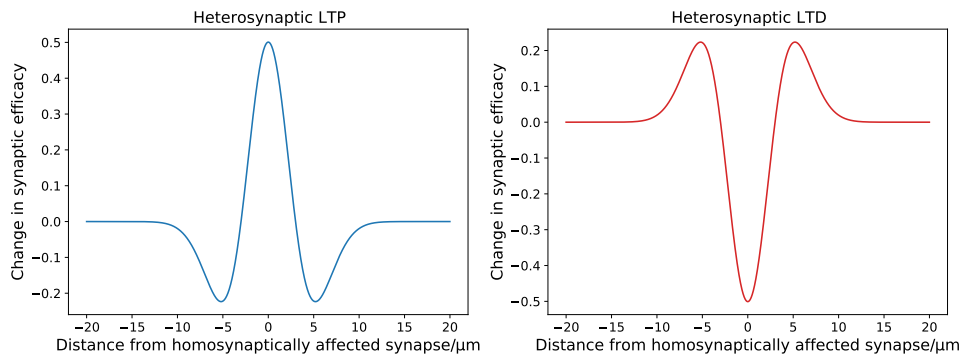


Figure 2.6.: In the above figures, two potential scenarios of heterosynaptic plasticity distribution are presented. The x-axis represents the distance of neighboring synapses from a homosynaptically stimulated synapse, which has a distance of 0 relative to itself. **Left:** The homosynaptically stimulated synapse undergoes LTP. It induces spatially weakening LTP on nearby neighboring synapses, followed by LTD on the remaining synapses that are in its window of influence. **Right:** The homosynaptically stimulated synapse undergoes LTD. It acts similarly to the LTP case except that the spatial sequence of LTP and LTD are reversed.

### Intracellular tetanization-induced heterosynaptic plasticity

Moreover, experiments were conducted using intracellular tetanization as a means to depolarise and evoke postsynaptic firing. These experiments involved no presynaptic stimulus and hence, any plasticity effects observed can be accounted to be entirely heterosynaptic [33, 17, 18, 16]. Besides the existence of heterosynaptic plasticity, the experiments also lead to conclusions about the direction of change of synaptic plasticity under such an induction protocol. The primary conclusion was that the direction of heterosynaptic change

## 2. Background

---

depended probabilistically on the weight of a particular synapse. An already potentiated synapse exhibited a tendency to depress while an already depressed synapse showed a tendency to potentiate.

Incorporation of such observations in computational models can be seen in the plasticity model published in [15]. A compartmental model with multiple ion channels was used to simulate the neuron. The model includes multiple fast currents including a fast calcium current,  $I_{Ca}$ . The dynamics of the calcium concentration are derived from this current, as shown in equation 2.15.

$$\frac{d[Ca]}{dt} = -AI_{Ca} - \frac{([Ca] - [Ca]_{max})}{\tau_{Ca}} \quad (2.15)$$

where:

- $A$  represents the coefficient that determines the spike in calcium concentration due to a calcium current of 1 unit at any particular point in time
- $[Ca]$  represents the concentration of  $Ca^{2+}$  ions
- $[Ca]_{max}$  represents the equilibrium calcium concentration
- $\tau_{Ca}$  represents the decay constant for the calcium concentration

The concentration of  $Ca^{2+}$  is used as an indicator for postsynaptic heterosynaptic change. Once the concentration of calcium in the postsynaptic neuron exceeds a certain threshold, the probability of a synapse undergoing a plastic change is calculated using equation 2.16.

$$P_i = 3000(w_i - \frac{w_{max}}{2})^2 + 0.1 \quad (2.16)$$

where:

- $P_i$  represents the probability of heterosynaptic change at synapse i
- $w_i$  represents the current weight of synapse i
- $w_{max}$  represents the maximum weight that a synapse can have

If  $P_i$  is greater than a random number generated from a uniform distribution from 0 and 1, the synapse undergoes heterosynaptic change given by the equation 2.17.

$$\Delta w_i = 0.0001 \left( \frac{1}{1 + \exp(100(w_i - 0.5w_{max}))} - 0.5 \right) + 0.02\sigma \quad (2.17)$$

where:

- $\sigma$  represents a random variable drawn from a Gaussian distribution with mean equalling 0 and a standard deviation of 3

#### Roles of heterosynaptic plasticity

Heterosynaptic plasticity rules discussed above may perform multiple functional roles. Firstly, in the discussion for rate-based models in section 2.2.4, we discussed how the BCM rule uses a sliding window to counteract the positive feedback loop that is characteristic of Hebbian-learning rules. Heterosynaptic plasticity of the type discussed above provides a more generalized mechanism to prevent such effects. In [5], it was shown that such heterosynaptic cooperation tends to counteract saturation of synaptic weights to  $w_{max}$ , preventing runaway synaptic dynamics. This allows a wider range of learning rules and activity patterns to be encoded into learning networks while maintaining the network in unsaturated configurations. Secondly, the heterosynaptic rules contribute to the enhanced synaptic competition. Competition amongst synapses can indeed be observed in purely homosynaptic plasticity rules, such as STDP, under appropriate input patterns. Nonetheless, additional heterosynaptic plasticity inflates the synaptic segregation between  $w_{min}$  and  $w_{max}$  and synapses reach a stable competitive configuration in fewer repetitions of a particular input pattern [5].

#### Spike-Timing-Dependent heterosynaptic plasticity [28]

A recent paper [28] investigated spike-timing-dependent heterosynaptic plasticity in layer 5 pyramidal neurons in juvenile mice. In [28], multiple experiments were conducted where either a single synapse was presynaptically activated or two synapses were co-activated simultaneously. It was shown that when LTP was induced on two synapses simultaneously, both synapses exhibited a greater tendency to potentiate in comparison to single synapse induction, given that the synapses were less than 5 micrometers apart. On the other hand, in the case of LTD, synapses co-stimulated along with the additional constrain that the synapses were no less than 40 micrometers apart, the synapses showed no LTD.

**LTP induction:** To induce t-LTP, repetitive spike-timing protocol (40 times, 0.5 Hz) in which 2P uncaging of glutamate at a single spine was closely followed in time (+7 or +13 ms) by a backpropagating AP (bAP) [28]. Changes in membrane potential due to the induction were monitored for 40 minutes. It was demonstrated that a repetitive pre-post pairing protocol of +13 ms reliably induced LTP but no changes were observed in the case when the bAP was induced +7ms after the glutamate uncaging. This indicates that the LTP has a preferential window in terms of the difference in timing between the presynaptic and postsynaptic stimulation (pre-post difference). When the same LTP induction procedure was applied to two synapses at the same time, something interesting was observed. Given that the spines under consideration were no more than 5 micrometers apart, the spines now were able to exhibit LTP when the pre-post difference was at +7ms. Therefore, indicating some form of heterosynaptic cooperation between the two spines.

**LTD induction:** LTD was studied using a repetitive spike-timing protocol in which 2P

## *2. Background*

---

uncaging of glutamate at a single spine was preceded in time by a bAP (post-pre protocol). When postsynaptic spikes preceded presynaptic firing by 15 ms (i.e., -15 ms), a significant reduction of the membrane potential amplitude occurred within minutes following LTD induction, and the spine underwent depression. When the same LTD induction procedure was applied to two synapses simultaneously, and the spines were less than 40 micrometers apart, the LTD was shut off, again indicating some mechanism of heterosynaptic cooperation.

In the following chapter, we use the experimental observations described in this subsection to develop our STDP model that incorporates similar heterosynaptic effects. We analyze the effects of some of the parameters in the model and how the synapses evolve under certain input patterns. Although we cannot specify the exact effects that such heterosynaptic cooperativity has on the functional properties of the individual synapses, the analyses we provide serve as a foundation for future development and work.

## **Part II.**

# **Pair-based STDP with Heterosynaptic Cooperativity**



### 3. Pair-based STDP with Heterosynaptic Cooperativity

#### 3.1. Modeling heterosynaptic cooperativity in co-activated spines

The model presented in this section extends the standard pair-based STDP model, described in section 2.2.5 to include heterosynaptic cooperativity observed experimentally in [28], and introduced in section 2.3.1.

##### 3.1.1. Heterosynaptic cooperativity

In order to capture cooperativity between synapses, the synapse model includes an additional local variable,  $\theta$ , that tracks the influence that synapses have on each other. More precisely,  $\theta_i$  tracks the cooperativity that neighboring synapses impose on synapse i. The differential equation that determines the dynamics of  $\theta_i$  are determined by equation 3.1.

$$\dot{\theta}_i(t) = -\frac{\theta_i(t)}{\tau_\theta} + \sum_{\forall k \neq i} w_i w_k \sum_{\forall j} \delta(t - t_{k,pre}^{(j)}) \exp\left(-\frac{|x_i - x_k|}{\lambda_{dist}}\right) \exp\left(-\frac{|t_{i,pre}^{(last)} - t_{k,pre}^{(j)}|}{\tau_{delay}}\right) + \sum_{\forall k \neq i} w_i w_k \sum_{\forall j} \delta(t - t_{i,pre}^{(j)}) \exp\left(-\frac{|x_i - x_k|}{\lambda_{dist}}\right) \exp\left(-\frac{|t_{i,pre}^{(j)} - t_{k,pre}^{(last)}|}{\tau_{delay}}\right) \quad (3.1)$$

where:

- $\theta_i(t)$  represents synaptic cooperativity at spine i
- $\tau_\theta$  represents the decay constant for heterosynaptic cooperativity
- $t_{i,pre}^{(j)}$  represents the arrival time of j-th presynaptic input at synapse k
- $t_{i,pre}^{(last)}$  represents the arrival time of the temporally nearest presynaptic spike at synapse i at time t with  $t_{i,pre}^{(last)} < t$
- $x_i$  represents the distance of synapse i relative to the neuronal cell body or soma
- $\lambda_{dist}$  represents the decay constant for the spatial decay of cooperativity

### 3. Pair-based STDP with Heterosynaptic Cooperativity

---

- $\tau_{delay}$  represents the decay constant for the temporal decay of cooperativity

Equation 3.1 captures the idea that when two or more synapses that are within a certain proximity of each other, are stimulated together (co-activated within a time window of less than 2ms, for example), they heterosynaptically cooperate to enhance potentiation and reduce depression. For example, if synapse k and synapse i are both stimulated at times  $t$  and  $t+\delta t$ , this would produce a spike in the heterosynaptic cooperativity of both synapses. This spike is scaled as a function of the distance between spine i and spine k ( $|x_i - x_k|$ ), as well as the difference in timing between the presynaptic input at spine k and last presynaptic input at spine i. A large intersynapse distance would result in a smaller spike in  $\theta_i$ . Similarly, a large temporal gap between the presynaptic spike timings would result in a smaller spike. The relationship is illustrated in the figure 3.1.

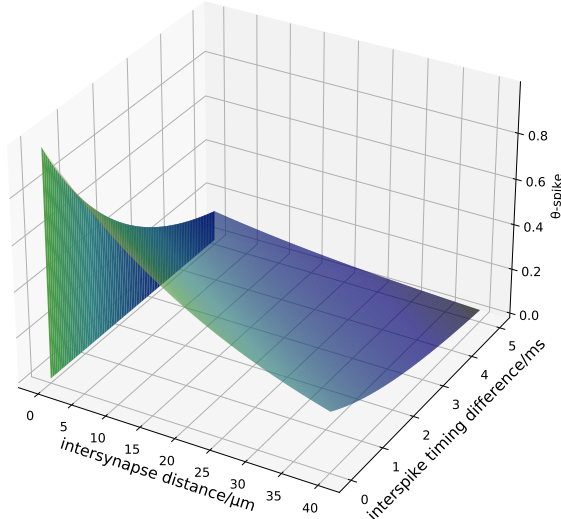


Figure 3.1.: Magnitude of synaptic cooperativity ( $\theta$ ) spike as a function of distance between co-activated synapses and the difference in timing of the presynaptic inputs at the synapses.

In order to break down the 3.1 further, we investigate the two summation terms on the right-hand side.

The first double summation depicts the case where a synapse k, that is a neighbor to

synapse  $i$ , is stimulated and causes the accumulation of cooperativity at synapse  $i$ . The term  $\sum_{\forall k \neq i}$  enforces this mechanism on all neighboring synapses and the term  $\sum_{\forall j}$  enforces it on all presynaptic spikes at the neighbors. The delta function captures the arrival of a presynaptic spike at a neighbor  $k$ , the first exponential term captures the idea that the cooperativity that a synapse can induce on a neighbor decays exponentially with the distance between them ( $|x_i - x_k|$ ) and similarly the second exponential term captures the idea that the cooperativity induction decreases exponentially with increasing difference between the latest presynaptic spike timings at two synapses ( $|t_{i,pre}^{(last)} - t_{k,pre}^{(j)}|$ ). The second summation is very similar to the first except that it depicts the case where a synapse  $i$  itself is stimulated and accumulates cooperativity due to previously arrived presynaptic spikes at its neighbors.

### 3.1.2. Spike-Timing-Dependent Plasticity (STDP) with heterosynaptic cooperativity

In order to include heterosynaptic cooperativity into the pair-based STDP model, introduced in 2.2.5, we augment the kernels in equation 2.12 with additional  $\theta$ -dependent factors,  $H_{LTP}$  and  $H_{LTD}$ .

$$\begin{aligned}\dot{w}_i(t) = & H_{LTP}(\theta_i(t)) A_{LTP} \sum_{\forall j} \delta(t - t_{post}^{(j)}) K(t_{post}^{(j)} - t_{i,pre}^{(last)}) \\ & + H_{LTD}(\theta_i(t)) A_{LTD} \sum_{\forall j} \delta(t - t_{i,pre}^{(j)}) K(t_{i,pre}^{(j)} - t_{post}^{(last)})\end{aligned}\quad (3.2)$$

$$H_{LTP}(\theta) = B_{LTP} + I_{LTP}(1 - \exp(-\alpha\theta)) \quad (3.3)$$

$$H_{LTD}(\theta) = B_{LTD} - D_{LTD}(1 - \exp(-\beta\theta)) \quad (3.4)$$

where:

- $B_{LTP}$  represents baseline LTP pre-factor with no heterosynaptic cooperativity (=1 in general)
- $I_{LTP}$  represents maximum possible increase in LTP due to heterosynaptic cooperativity ( $I_{LTP} \geq 0$ )
- $\alpha$  represents the parameter that defines the decaying relationship between heterosynaptic LTP and  $\theta$
- $B_{LTD}$  represents baseline LTD pre-factor with no heterosynaptic effects (=1 in general)
- $D_{LTD}$  represents maximum possible decrease in LTD due to heterosynaptic cooperativity ( $0 \leq D_{LTD} \leq 1$ )

### 3. Pair-based STDP with Heterosynaptic Cooperativity

---

- $\beta$  represents the parameter that defines the decaying relationship between heterosynaptic LTD and  $\theta$

Qualitatively, we model  $H_{LTP}(\theta)$  to increase with  $\theta$  and level off at a certain point in order to prevent uncontrolled potentiation (representing some form of resource limitation). On the other hand,  $H_{LTD}(\theta)$  behaves slightly differently. As described in [28], synaptic cooperation results in switching off of depressive behavior and hence  $H_{LTD}(\theta)$  rapidly moves to zero as  $\theta$  increases. This is illustrated in figure 3.2.

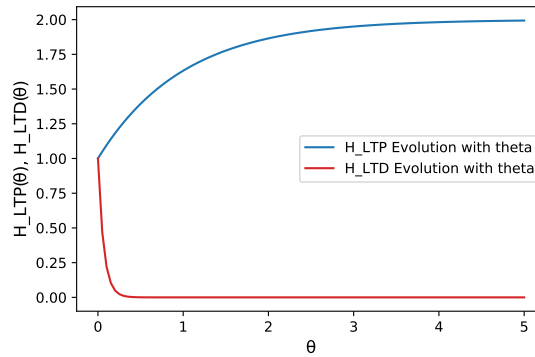


Figure 3.2.: With no synaptic cooperativity ( $\theta = 0$ ),  $H_{LTP}$  and  $H_{LTD}$  have baseline values of 1 and 1 respectively. As  $\theta$  increases, both factors increase with  $H_{LTP}$  levelling off at 2 and  $H_{LTD}$  at 0. Note that the change in  $H_{LTD}$  up to the zero level is much faster than the change in  $H_{LTP}$ . This captures the idea that even for small values of  $\theta$  (large distance between synapses) depression is turned off while the effects of cooperativity on the LTP side are active only for large  $\theta$  values (small distance between synapses). The parameters used in the illustration above are  $B_{LTP} = 1$ ,  $I_{LTP} = 1$ ,  $\alpha = 1$ ,  $B_{LTD} = 1$ ,  $D_{LTD} = 1$ , and  $\beta = 10$ .

On a higher level of abstraction, we can analyze the dependence of  $H_{LTP}$  and  $H_{LTD}$  on intersynapse distance in the case where both synapses are simultaneously stimulated. The qualitative behavior follows that for small distances  $H_{LTP}$  for the stimulated synapses is high when they are clustered and decays back to baseline amplitude as the intersynapse distance increases. For  $H_{LTD}$ , at small intersynapse distances amplitude is very close to 0 to mimic suppression of depression and as distance increases the amplitude returns to the baseline. This is illustrated in figure 3.3.

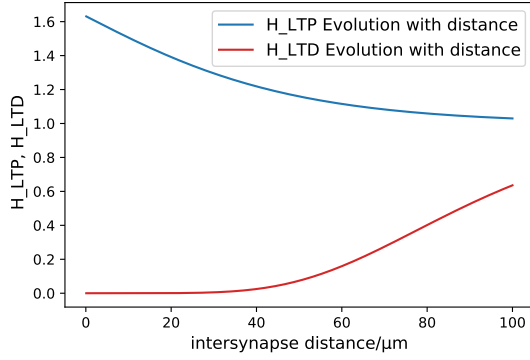


Figure 3.3.:  $H_{LTP}$  and  $H_{LTD}$  amplitudes as a function of intersynapse distance in the case where two synapses are **simultaneously stimulated**. The parameters used in the illustration above are  $B_{LTP} = 1$ ,  $I_{LTP} = 1$ ,  $\alpha = 1$ ,  $B_{LTD} = 1$ ,  $D_{LTD} = 1$ , and  $\beta = 10$ .

### 3.1.3. Effects of heterosynaptic cooperativity on the STDP kernel

In this subsection we illustrate the effect of the heterosynaptic factors  $H_{LTP}(\theta)$  and  $H_{LTD}(\theta)$  on the STDP kernels. Figures 3.4 and 3.5 show the effect of different values of  $\theta$  on the E-kernel and the G-kernel respectively.

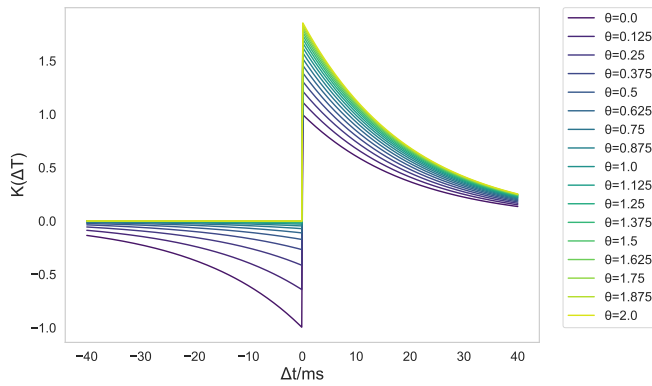


Figure 3.4.: The illustration above shows the changes in the E-kernel when augmented with the heterosynaptic factor. Each plot represents the kernel for a different value of theta. The parameters used in the illustration above are  $B_{LTP} = 1$ ,  $I_{LTP} = 1$ ,  $\alpha = 1$ ,  $B_{LTD} = 1$ ,  $D_{LTD} = 1$ , and  $\beta = 2.5$ .

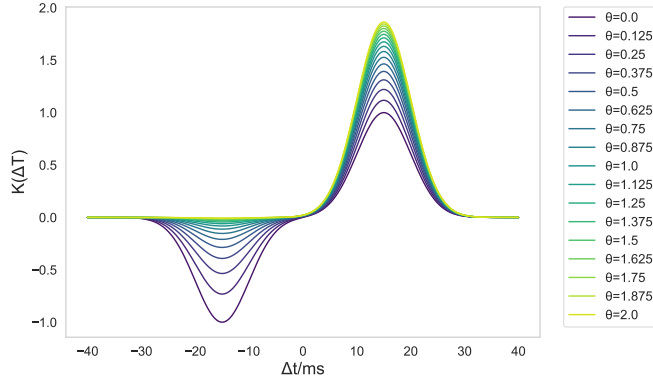


Figure 3.5.: The illustration above shows the changes in the G-kernel when augmented with the heterosynaptic factor. Each plot represents the kernel for a different value of theta. The parameters used in the illustration above are  $B_{LTP} = 1$ ,  $I_{LTP} = 1$ ,  $\alpha = 1$ ,  $B_{LTD} = 1$ ,  $D_{LTD} = 1$ , and  $\beta = 2.5$ .

## 3.2. Validation of heterosynaptic STDP with LTP drift

In order to validate the implementation, we demonstrate the characteristic positive drift of STDP models due to the causal relationship between excitatory presynaptic inputs and postsynaptic firing. More precisely, since presynaptic inputs transiently increase the probability of postsynaptic firing, a postsynaptic action potential is likely to follow shortly afterward and thus increases the chances of a pre-post pair and thus potentiation [2]. This average "drift" towards potentiation can be mitigated by strengthening the LTD window, particularly by allowing  $A_{LTD}$  to be greater than  $A_{LTP}$ . In the subsections below we provide the results of multiple simulations with and without heterosynaptic plasticity enabled (additional results in A.2). In each set of results, we present the drift of the mean synaptic weight for different values of  $A_{LTD}$  while keeping  $A_{LTP}$  constant.

### 3.2.1. Setup

The simulation setup involves a single LIF neuron consisting of a single dendrite of evenly spaced excitatory synapses (spacing is defined by the parameter *synaptic\_gap*). The dendrite consists of 80 synapses, each of which receives independent Poisson inputs of frequency 3.2 Hz from external sources. Moreover, the initial weight of each of the synapses is set to 1. The simulations are 5 seconds long. Figure 3.6 provides a visual illustration of the setup. Table 3.1 provides the set of parameters that are relevant to the simulations in this section.

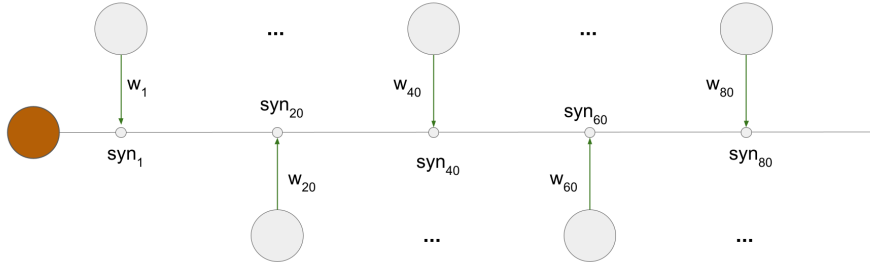


Figure 3.6.: The figure illustrates the setup for the LTP-drift experiments. We investigate a single LIF neuron with 80 excitatory synapses on its single dendrite. The synapses are uniformly separated with a gap of  $1\mu m$ . Each of the synapses receive a Poisson input firing at a frequency of 3.2 Hz, indicated by the green arrows.

Parameter	Value	Unit
<b>Simulation</b>		
simulation time	5.0	s
$dt$	0.0001	s
<b>LIF Neuron</b>		
$\tau_m$	0.02	s
$V_{rest}$	10	mV
$V_\theta$	20	mV
$\tau_{ref}$	0.002	s
<b>Uniform Connectivity</b>		
$synaptic\_gap$	1	$\mu m$
<b>Heterosynaptic Instantaneous Synapse</b>		
$J$	2.35	dmV/Spike
$\tau_\theta$	0.010	s
$\lambda_{dist}$	20.0	$\mu m$
$\tau_{delay}$	0.001	s
$w_{initial}$	1	-
$(w_{min}, w_{max})$	(0,2)	-
$(A_{LTP}, A_{LTD})$	(0.15,?)	-
$(B_{LTP}, B_{LTD})$	(1,1)	-
Normalization	Hardbound	-

Table 3.1.: Parameters for the STDP validation simulations that remain unchanged for all cases in this section. The synaptic parameters  $w_{initial}$ ,  $w_{max}$ , and  $w_{min}$  represent the initial weight for all synapses, the maximum weight that a synapse can potentiate to and the minimum weight that a synapse can depress to respectively. The "Normalization" parameter determines the mechanism used to ensure synaptic weights are always within the bounds of  $w_{min}$  and  $w_{max}$  (refer to A.1 for details).

### 3. Pair-based STDP with Heterosynaptic Cooperativity

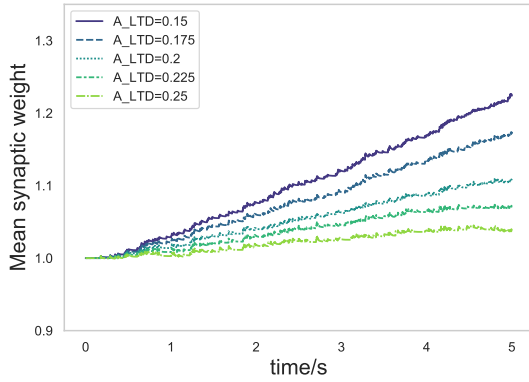
---

#### 3.2.2. Results and Discussion

In this section, we present the results for the setup described in 3.2.1. Each subsection contains a table of parameters that are relevant and specific to the particular set of simulations.

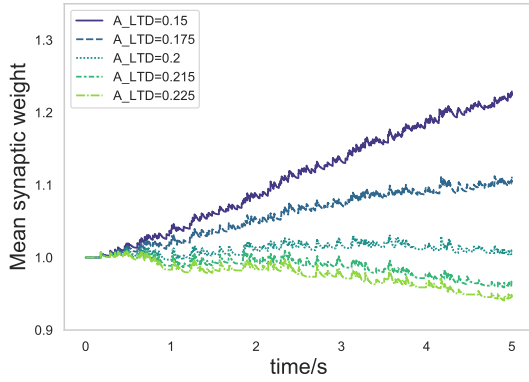
##### E-Kernel, G-Kernel with no Heterosynaptic Cooperativity

In this subsection, we explore the difference between the two STDP kernels we introduced in previous sections in terms of the prominence of the LTP drift and how sensitive the drift mitigation is to increasing values of  $A_{LTD}$ .



Parameter	Value	Unit
<b>Heterosynaptic Instantaneous Synapse</b>		
Kernel	E-Kernel	-
$\tau_{LTP}$	0.02	s
$\tau_{LTD}$	0.02	s
$A_{LTD}$	0.15, 0.175, 0.2, 0.225, 0.25	-
$(\alpha_{LTP}, \beta_{LTD})$	(0,0)	-

Figure 3.7.: **Left:** LTP drift for E-Kernel without heterosynaptic cooperativity. Increasing  $A_{LTD}$  reduces the LTP drift. **Right:** Parameters specific to the set of simulations.



Parameter	Value	Unit
<b>Heterosynaptic Instantaneous Synapse</b>		
Kernel	G-Kernel	-
$\mu_{LTP}, \sigma_{LTP}$	0.013, 0.035	s
$\mu_{LTD}, \sigma_{LTD}$	0.013, 0.035	s
$A_{LTD}$	0.15, 0.175, 0.2, 0.225, 0.25	-
$(\alpha_{LTP}, \beta_{LTD})$	(0,0)	-

Figure 3.8.: **Left:** LTP drift for G-Kernel without heterosynaptic cooperativity. Increasing  $A_{LTD}$  reduces the LTP drift. **Right:** Parameters specific to the set of simulations.

### 3.2. Validation of heterosynaptic STDP with LTP drift

Figures 3.7 and 3.8 show that increasing  $A_{LTD}$  reduces the LTP drift. It is apparent that the effect of increasing the magnitude of  $A_{LTD}$  is more prominent in the case of the G-Kernel, i.e., small increases in  $A_{LTD}$  push the mean of the synaptic weights to remain balanced around 1. In the E-Kernel, a postsynaptic action potential causes maximal potentiation on the synapse whose presynaptic spike is temporally nearest to a postsynaptic spike. On the other hand, the G-Kernel induces maximal potentiation on a synapse whose presynaptic spike is  $\mu_{LTP}$  behind the postsynaptic spike. Therefore, the causal relationship between a pre-post pair is less prominent in the case of the G-Kernel as there exists a larger temporal window for a pre-post pair to be offset by a post-pre pair.

#### Effect of $\alpha$ and $\beta$

In this subsection we demonstrate the sensitivity of the model to  $\alpha$  and  $\beta$ . These two parameters control the sensitivity of the augmented STDP kernels to  $\theta$ . Increasing the value of  $\alpha$  results in an increase in the LTP enhancement for the same level of heterosynaptic cooperation. Similarly, increasing the value of  $\beta$  results in an increase in the LTD suppression for the same level of heterosynaptic cooperation.

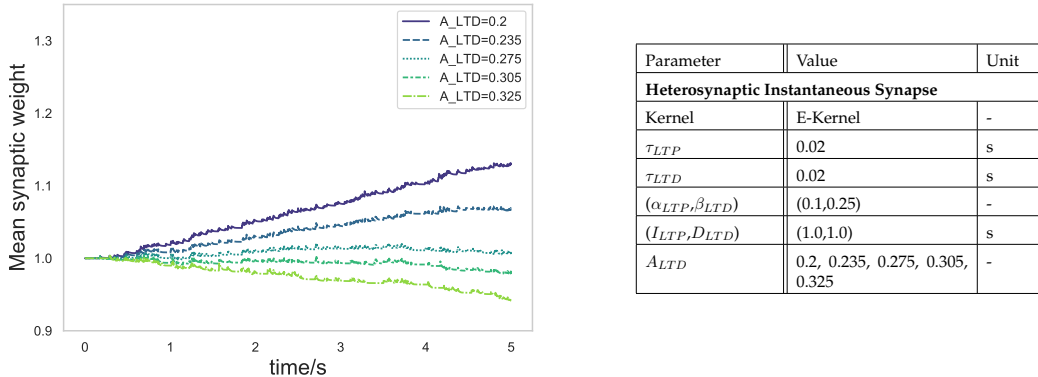


Figure 3.9.: **Left:** LTP drift for E-Kernel heterosynaptic cooperativity,  $\alpha_{LTP} = 0.1$ ,  $\beta_{LTD} = 0.25$ . **Right:** Parameters specific to the set of simulations.

The  $\alpha$  and  $\beta$  values used for simulations in figure 3.10 are 1.0 and 2.5 respectively, an order of magnitude higher than the values used in the cases presented in figure 3.9. Comparing the figures show clearly that higher values of  $\alpha$  and  $\beta$  increase the sensitivity of the model to  $\theta$  which equates to a higher LTP bias. Consequently, the magnitudes of  $A_{LTD}$  required to mitigate the LTP drift are noticeably higher.

### 3. Pair-based STDP with Heterosynaptic Cooperativity

---

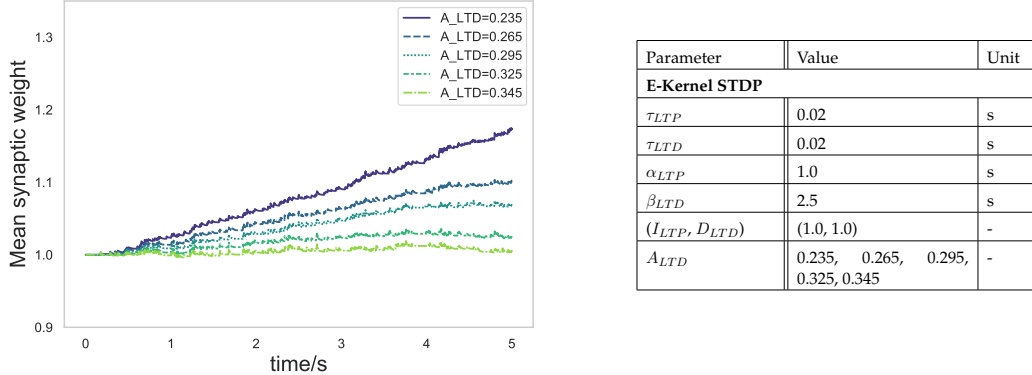


Figure 3.10.: **Left:** LTP drift for E-Kernel heterosynaptic cooperativity,  $\alpha_{LTP} = 1.0$ ,  $\beta_{LTD} = 2.5$ . **Right:** Parameters specific to the set of simulations.

#### Effect of $I_{LTP}$ and $D_{LTP}$

In this subsection we demonstrate the sensitivity of the model to  $I_{LTP}$  and  $D_{LTP}$ .  $I_{LTP}$  represents the maximal possible increase of the peak LTP response of the STDP kernel in response to high levels of cooperativity whereas  $D_{LTP}$  represents the maximal possible decrease of the peak LTD response of the STDP kernel in response to high levels of cooperativity.

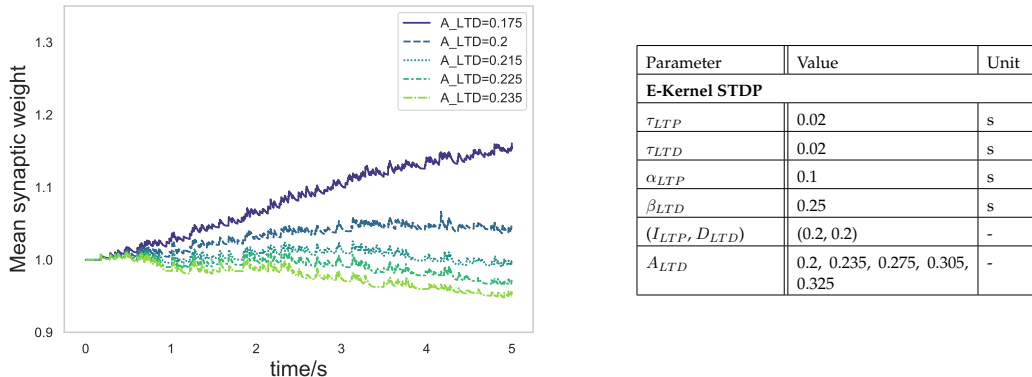


Figure 3.11.: **Left:** LTP drift for E-Kernel heterosynaptic cooperativity,  $I_{LTP} = 0.2$ ,  $I_{LTD} = 0.2$ . **Right:** Parameters specific to the set of simulations.

Comparison between the simulation results in figures 3.11 and 3.12 shows the increase in sensitivity of the model to cooperativity signals,  $\theta$ , with increase in the values of  $I_{LTP}$  and  $D_{LTP}$ . The values of  $I_{LTP}$  and  $D_{LTP}$  are higher for the simulations in 3.12 allowing

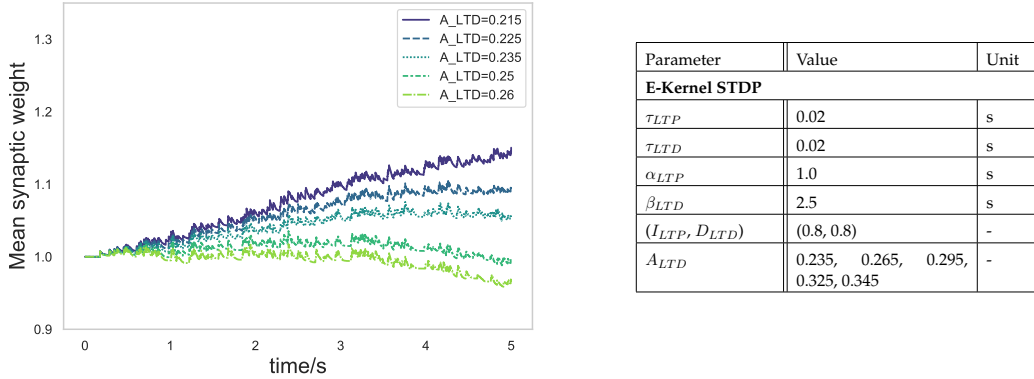


Figure 3.12.: **Left:** LTP drift for E-Kernel heterosynaptic cooperativity,  $I_{LTP} = 0.8$ ,  $I_{LTD} = 0.8$ . **Right:** Parameters specific to the set of simulations presented in the figure.

the STDP kernel to enhance potentiation and suppress depression more prominently in comparison to 3.11. Therefore, the LTP bias is higher for the simulations, and thus the magnitudes of  $A_{LTD}$  required to mitigate the LTP drift are noticeably larger.

### Visual analysis of heterosynaptic cooperativity, $\theta$

Figure 3.13 visualizes a typical instance of the evolution of cooperativity one each synapse under our heterosynaptic rule. The markers on the figure indicate spikes in cooperativity due to the coincidence of presynaptic inputs at different synapses. These spikes in cooperativity can be interpreted as fluctuations in  $Ca^{2+}$  concentration at the synaptic cleft which facilitates potentiation and suppresses depression. The phenomenon has similarities with the Graupner model, introduced in section 2.2.5. Recalling the foundations of the Graupner model, high concentrations of intracellular  $Ca^{2+}$  concentrations resulted in LTP in comparison, whereas moderate concentrations resulted in LTD. Similarly, in our rule, the STDP kernel morphs into an LTP-biased system when high cooperation between synapses raises  $Ca^{2+}$  concentrations, indicated by spikes in  $\theta$ .

Multiple parameters affect the magnitude and the persistence of cooperativity. From equation 3.1, increasing  $\tau_\theta$  would result in longer persistence of the theta spikes in figure 3.13. Moreover, increasing  $\lambda_{dist}$  and  $\tau_{delay}$  would result in larger cooperativity spikes. Increasing the former would allow spatially further neighboring synapses to impose cooperativity over a particular synapse, whereas increasing the latter increases the window of coincidence between presynaptic spikes at two different synapses.

Additionally, figure 3.14 illustrates the spikes at a particular synapse due to the coincidence of nearly coincident inputs at the synapse under consideration and one or more of its neighbors.

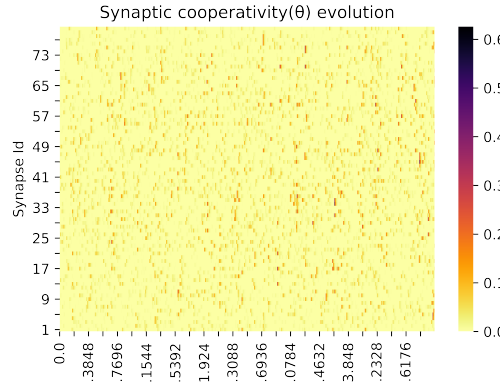


Figure 3.13.: Example  $\theta$  evolution for each synapse averaged over 5 runs.

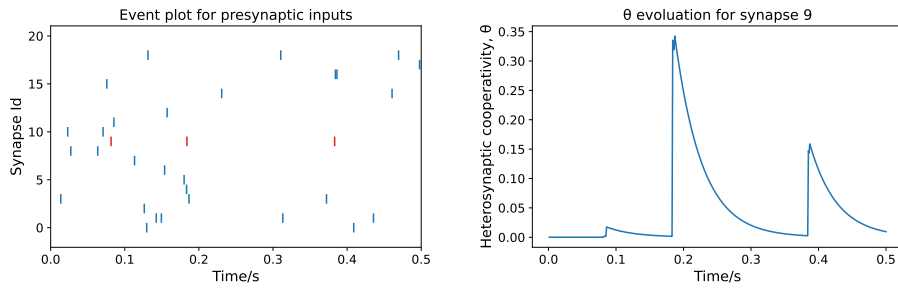


Figure 3.14.: Example  $\theta$  spikes synapse with id 9 due to coincident spikes at the synapse and one or more of its neighbors. **Left:** Event plot of presynaptic input spikes at each of 20 synapses that are considered. **Right:** Local  $\theta$  spikes at synapse 9. The presynaptic input at synapse 9 around the 0.2 s point coincides with more neighboring presynaptic spikes in comparison to the spikes around the 0.1 s and 0.4 s marks. This is reflected in the larger magnitude of the  $\theta$  spike at the 0.2 s mark.

### 3.3. Spatial effects of Heterosynaptic Cooperativity

In this section, we explore the spatial effects that synapses have on their neighbors due to our heterosynaptic rule using a second simulation setup.

#### 3.3.1. Setup

The simulation setup involves a single neuron consisting of a single dendrite of evenly spaced excitatory synapses (spacing is defined by the parameter *synaptic\_gap*). In order to reduce variability, we configure our neuron to spike at a constant rate at a frequency of 4 Hz. The dendrite consists of 1000 synapses, each of which receives an independent Poisson input of 10 Hz. The simulations are 30, 50, or 70 seconds long, depending on the time taken for the synaptic weights to reach a stable distribution. Figure 3.15 provides a

visual illustration of the setup. In addition, 3.2 provides the parameter set that remains unchanged for all simulations presented in this section.

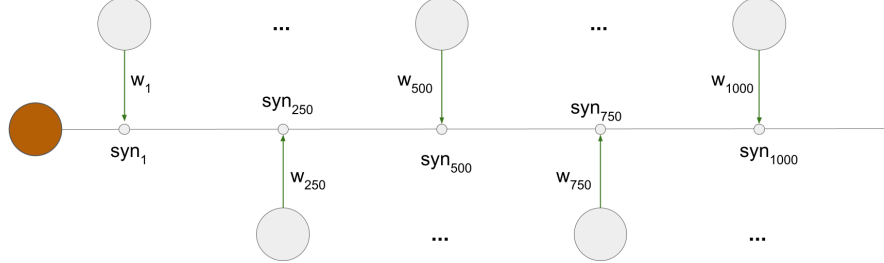


Figure 3.15.: The figure illustrates the experimental setup for the spatial analysis of cooperativity. We configure a single neuron with a fixed Poisson firing rate of 4 Hz with 1000 excitatory synapses on its single dendrite. The synapses are uniformly separated with a gap of  $0.5\mu m$ . Each of the synapses receive a Poisson input firing at a frequency of 10.0 Hz, indicated by the green arrows.

In contrast to the simulation setup in section 3.2.1, in this case, the weights are not homogeneously initialized to 1. Instead, we initialize the weights to either 1 or  $w_{max} = 2$  in order to create boundaries in the weight distribution. In the subsequent sections, we present the results of 3 different configurations of the initial weight distribution. These configurations are presented in figure 3.16. We refer to the bands of synapses that are initially maximal as maximal bands and ones initialized to 1 as the median bands. In addition, table 3.2 provides the set of parameters that are relevant to the simulations in this section.

### 3. Pair-based STDP with Heterosynaptic Cooperativity

---

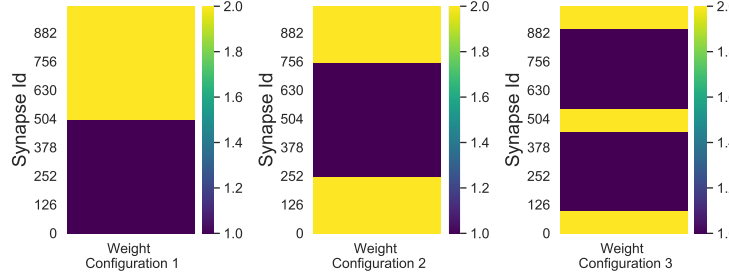


Figure 3.16.: The figure illustrates the different weight distributions used to create heterogeneous weight boundaries. **Left:** Configuration 1 initializes the first 500 synapses to  $w_{min}$  (median band) and the second 500 synapses to  $w_{max}$  (maximal band). **Middle:** Configuration 2 initializes the first 250 synapses to  $w_{max}$  (first maximal band), the next 500 synapses to  $w_{min}$  (median band) and the last 250 synapses to  $w_{max}$  (second maximal band). **Right:** Configuration 3 initializes the first 100 synapses, the last 100 synapses and 100 synapses in the middle to  $w_{max}$  (maximal bands) and the rest are initialized to  $w_{min}$  (median bands).

Parameter	Value	Unit
<b>Simulation</b>		
simulation time	30.0	s
$dt$	0.0001	s
<b>Poisson Neuron</b>		
firing rate	4	Hz
<b>Dendrite</b>		
<i>synaptic_gap</i>	0.5	$\mu\text{m}$
<b>Heterosynaptic Instantaneous Synapse</b>		
$J$	0	dmV/Spike
$\tau_\theta$	0.025	s
$\lambda_{dist}$	30.0	$\mu\text{m}$
$\tau_{delay}$	0.001	s
$(I_{LTP}, D_{LTD})$	(1,1)	-
$(w_{min}, w_{max})$	(0,2)	-
Normalization	Hardbound	-
<b>STDP</b>		
Kernel	E-Kernel	-
$(A_{LTP}, A_{LTD})$	(1.2,1.2)	-
$(\alpha_{LTD}, \beta_{LTD})$	(5.0,15.0)	-
$(B_{LTP}, B_{LTD})$	(?,1.0)	-

Table 3.2.: Parameters for the spatial analysis simulations that remain unchanged for all cases in this section.

### 3.3.2. Results - Configuration 1

**E-Kernel with  $B_{LTP} = 0.75$**

In the non-heterosynaptic case presented in 3.17, the synaptic weights stabilize below 1 since the parameter set produces an overall LTD bias. If we observe the depression of the maximal band, there is no apparent pattern in this process, which is expected since we have no cooperativity between the synapses and they each depress in a random manner.

On the other hand, the heterosynaptic case presented in 3.18, the parameter set imposes an LTP bias and the mean weight saturates to the maximum. As for the potentiation of the median band, it is vaguely observable that synapses further away from the maximal band saturate more slowly in comparison to the synapses that are spatially nearer.

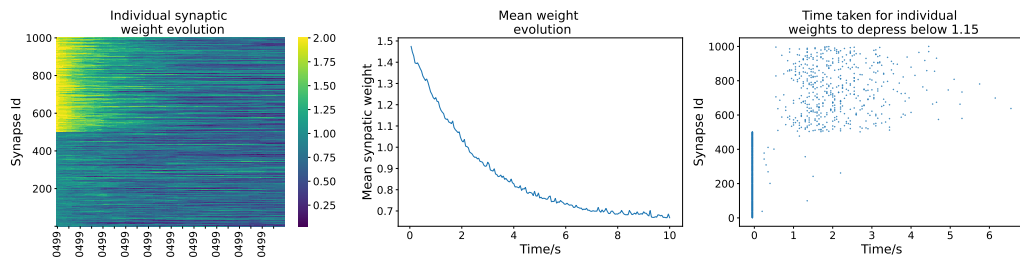


Figure 3.17.: E-Kernel simulation without heterosynaptic cooperativity. The figures present data averaged over 10 runs with different seeds. **Left:** Figure shows the evolution of individual synaptic weights over the course of the simulation. **Middle:** Figure shows the evolution of the mean synaptic weight. The scenario is LTD dominant and the mean of the weights stabilises below 1. **Right:** Figure shows the time taken by each of the synaptic weights to depress below 1.15.

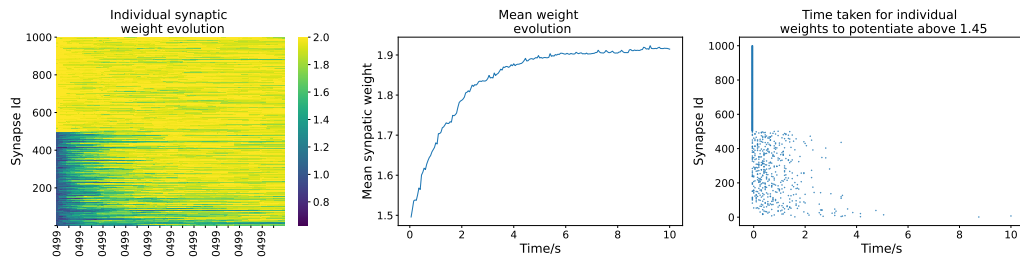


Figure 3.18.: E-Kernel simulation with heterosynaptic cooperativity,  $B_{LTP} = 0.75$ . The figures present data averaged over 10 runs with different seeds. **Left:** Figure shows the evolution of individual synaptic weights over the course of the simulation. **Middle:** Figure shows the evolution of the mean synaptic weight. The scenario is LTP dominant and the mean of the weights stabilises around 2. **Right:** Figure shows the time taken by each of the synapse weights to potentiate above 1.45.

### 3. Pair-based STDP with Heterosynaptic Cooperativity

---

**E-Kernel,  $B_{LTP} = 0.0$**

In order to confirm our observation from the previous section, we set up a more extreme simulation with  $B_{LTP} = 0.0$ , meaning that no LTP exists without heterosynaptic cooperativity. Again, in the non-heterosynaptic case illustrated in figure 3.19, the synapses depress to 0 in a random fashion.

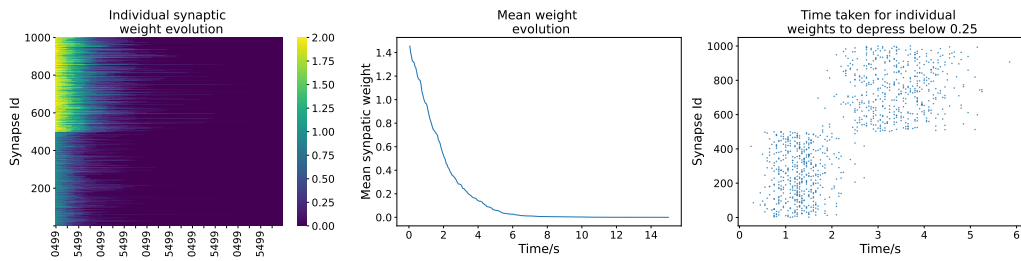


Figure 3.19.: E-Kernel simulation without heterosynaptic cooperativity. The figures present data averaged over 10 runs with different seeds. **Left:** Figure shows the evolution of individual synaptic weights over the course of the simulation. **Middle:** Figure shows the evolution of the mean synaptic weight. The scenario is LTD dominant and the mean of the weights stabilises below 0. **Right:** Figure shows the time take by each of the synapse weights to drop below 0.25.

On the other hand, in the heterosynaptic case illustrated in figure 3.20, it is distinctly visible that synapses in the median band that are closer to the maximal band experience a slower depression process since they cooperate more strongly with the initially potentiated maximal band synapses.

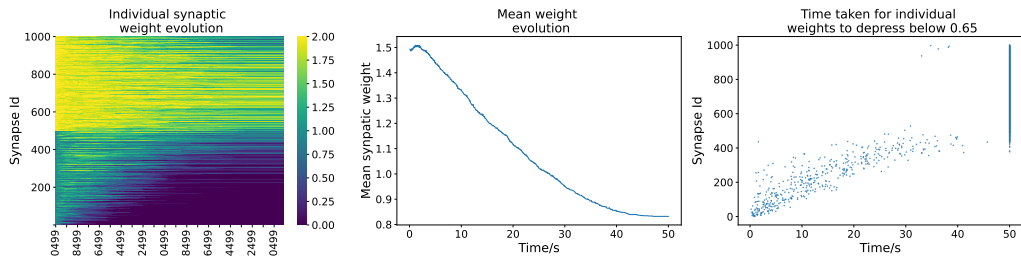


Figure 3.20.: E-Kernel simulation with heterosynaptic cooperativity,  $B_{LTP} = 0.0$ . The figures present data averaged over 10 runs with different seeds. **Left:** Figure shows the evolution of individual synaptic weights over the course of the simulation. **Middle:** Figure shows the evolution of the mean synaptic weight. The scenario is LTD dominant and the mean of the weights stabilises below 0. **Right:** Figure shows the time take by each of the synapse weights to drop below 0.65.

### 3.3.3. Results - Configuration 2

**E-Kernel**,  $B_{LTP} = 0.0$

Similar to configuration 1, spatial effects of our heterosynaptic rule are visible in the case of configuration 2 as well. The non-heterosynaptic case illustrated in figure 3.21 shows a random decay of synaptic weights.

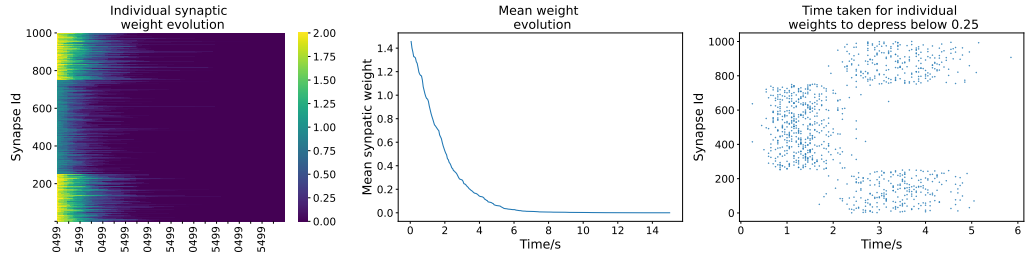


Figure 3.21.: E-Kernel simulation without heterosynaptic cooperativity. The figures present data averaged over 10 runs with different seeds. **Left:** Figure shows the evolution of individual synaptic weights over the course of the simulation. **Middle:** Figure shows the evolution of the mean synaptic weight. The scenario is LTD dominant and the mean of the weights stabilises below 0. **Right:** Figure shows the time take by each of the synapse weights to drop below 0.25.

However, the heterosynaptic case shown in figure 3.22 confirms the observation where synapses in median bands that are spatially nearer to neighboring maximal bands cooperate strongly with the maximal band synapses and depress at a lower rate towards the fully depressed state.

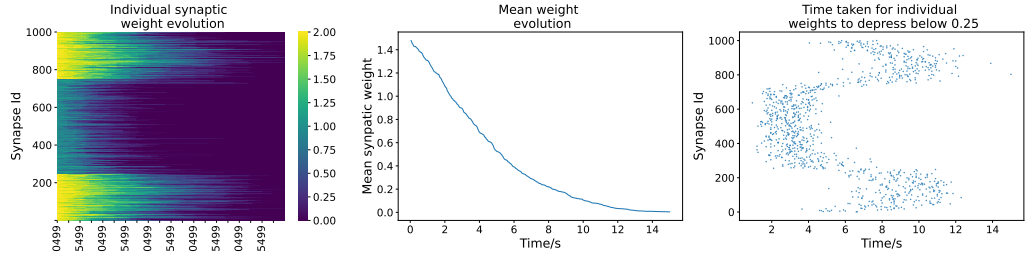


Figure 3.22.: E-Kernel simulation with heterosynaptic cooperativity,  $B_{LTP} = 0.0$ . **Left:** Figure shows the evolution of individual synaptic weights over the course of the simulation. The figures present data averaged over 10 runs with different seeds. **Middle:** Figure shows the evolution of the mean synaptic weight. The scenario is LTD dominant and the mean of the weights stabilises below 0. **Right:** Figure shows the time take by each of the synapse weights to drop below 0.25.

### 3.3.4. Results - Configuration 3

The observations for configuration 3 are similar to that for the previous configurations. The figures 3.23 and 3.24 serve as illustrations for these observations.

**E-Kernel,  $B_{LTP} = 0.0$**

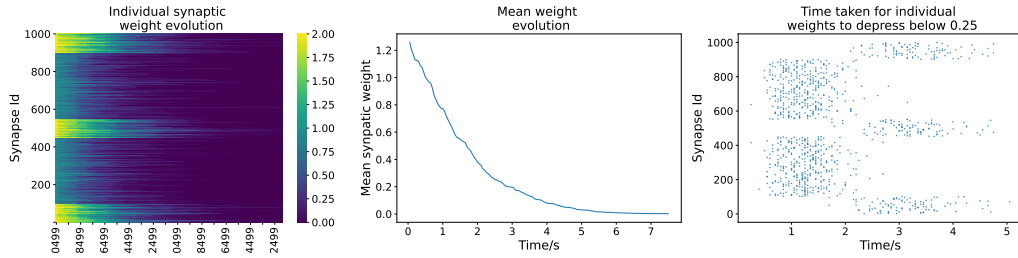


Figure 3.23.: E-Kernel simulation without heterosynaptic cooperativity. The figures present data averaged over 10 runs with different seeds. **Left:** Figure shows the evolution of individual synaptic weights over the course of the simulation. **Middle:** Figure shows the evolution of the mean synaptic weight. The scenario is LTD dominant and the mean of the weights stabilises below 0. **Right:** Figure shows the time take by each of the synapse weights to drop below 0.25.

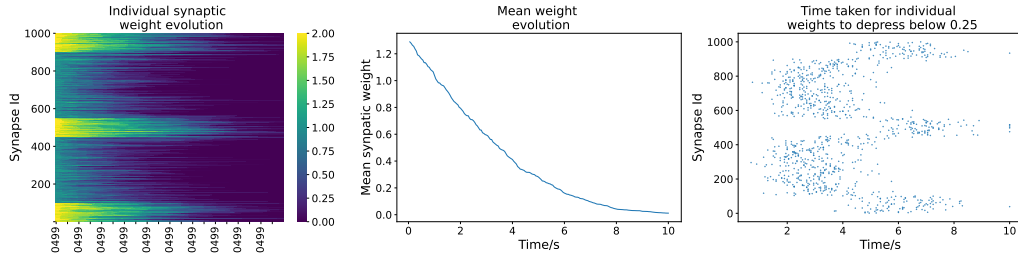


Figure 3.24.: E-Kernel simulation with heterosynaptic cooperativity,  $B_{LTP} = 0.0$ . The figures present data averaged over 10 runs with different seeds. **Left:** Figure shows the evolution of individual synaptic weights over the course of the simulation. **Middle:** Figure shows the evolution of the mean synaptic weight. The scenario is LTD dominant and the mean of the weights stabilises below 0. **Right:** Figure shows the time take by each of the synapse weights to drop below 0.25.

## 3.4. Implementation overview

In this section, we discuss certain details of our implementation including the existing execution framework, additional heterosynaptic constructs that were implemented, the time-stepping scheme for the ODEs, etc.

### 3.4.1. Network execution framework

The most important classes or constructs in the implementation include the NeuronPop, Connectivity, Synapse, and Stimulus classes. The listing below along with 3.25 provides details regarding these three classes.

- **NeuronPop:** Stores a vector of neurons that belong to a particular population. An additional vector tracks the membrane potentials of each of the neurons. In each timestep of the simulation, the *advect* method is called (with the input currents for each neuron as a parameter) on each instance of NeuronPop in order to update the membrane potential of the neurons and to determine a list of neurons that have spiked in that step.
- **Connectivity:** Determines the scheme used to connect neurons of two different (or same in case of recurrent connections) populations. Therefore, for each pair of NeuronPop instances, there exists a Connectivity instance. Moreover, Connectivity stores the source-target information for the neurons. Each Connectivity instance is contained in a Synapse instance.
- **Synapse:** Contains the connectivity information between two NeuronPop instances using a Connectivity instance as a member variable. In each timestep of the simulation, the *advect* method is called on each instance of Synapse and this populates a vector that stores the input current for the postsynaptic NeuronPop in the next timestep.
- **Stimulus:** There exists one Stimulus instance for each NeuronPop. In each time step, the *advect* method is called on each instance of Stimulus and this populates a vector that stores the *external* input current for the postsynaptic NeuronPop in the next timestep.

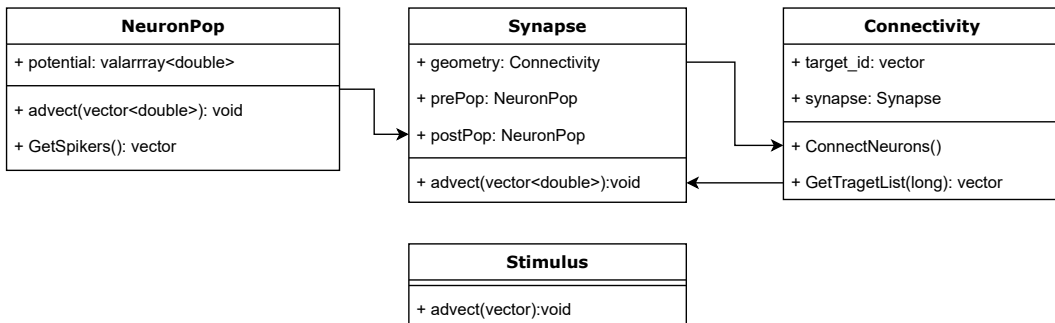


Figure 3.25.: Class diagrams for the NeuronPop, Synapse, Connectivity, and Stimulus. Only essential members and methods required for the discussion are included in the figure.

### 3. Pair-based STDP with Heterosynaptic Cooperativity

---

In addition, algorithm 1 provides an overview of how the simulations are set up and the execution is run.

---

#### Algorithm 1 Execution Framework

---

```
1: simTime ← length of simulation
2: dt ← timestep
3: time ← current time
4:
5: neuronPops ← vector of NeuronPop
6: stimulus ← vector of external stimulus for each NeuronPop
7: synapses ← vector of Synapse
8:
9: synapticDv ← 2D vector of input currents
10:
11: while time ≤ simTime do
12:   synapticDv = 0
13:
14:   for synId = 1, 2, . . . , S do
15:     synapses[synId].advect(synapticDv) // populate synaptic dv
16:   end for
17:
18:   for stim = 1, 2, . . . , N do
19:     stimulus[stim].advect(synapticDv) // populate synaptic dv
20:   end for
21:
22:   for popId = 1, 2, . . . , N do
23:     neuronPops[popId].advect(synapticDv) // consume synaptic dv
24:   end for
25:
26:   time = time + dt
27: end while
```

---

#### 3.4.2. Heterosynaptic Extensions

In order to incorporate heterosynaptic mechanisms into the framework, the base classes introduced in the previous section were extended. The listing below along with 3.26 provides details regarding these sub-classes.

- **AllocationState:** A struct that stores the dendritic state of a Neuron. Added to enable a mechanism for the implementation of different dendritic morphologies.
- **SynExt:** A struct that is used to store local synaptic information, such as cooperativity, efficacy as well as ids of pre and post-neurons.
- **HeteroNeuronPop:** Extends NeuronPop. At any point in time, HeteroNeuronPop stores a vector of synapses that have spiked in the previous timestep. This is used by each HeteroSynapse instance associated with the HeteroNeuronPop instance (HeteroSynapse instances for which the HeteroNeuronPop instance is the postsynaptic population) to update cooperativity between synapses. Additionally, each instance stores an AllocationState for each neuron in the population. This allows a new

synapse to be allocated on the dendritic tree of each neuron based on the allocation of the previous synapse; essentially providing a mechanism for the implementation of different dendritic geometries.

- **HeteroSynapse:** Extends Synapse. Reads a vector of spiked synapses from HeteroNeuronPop and updates the heterosynapses based on the rules of cooperativity. Furthermore, updates plasticity kernels or rules based on changes in cooperativity between synapses.
- **HeteroConnectivity:** Extends Connectivity. Provides the implementation for allocation of new synapses that may or may not depend on the AllocationState stored in NeuronPop. Contains a vector of SynExt, one for each neuron of the postsynaptic population.

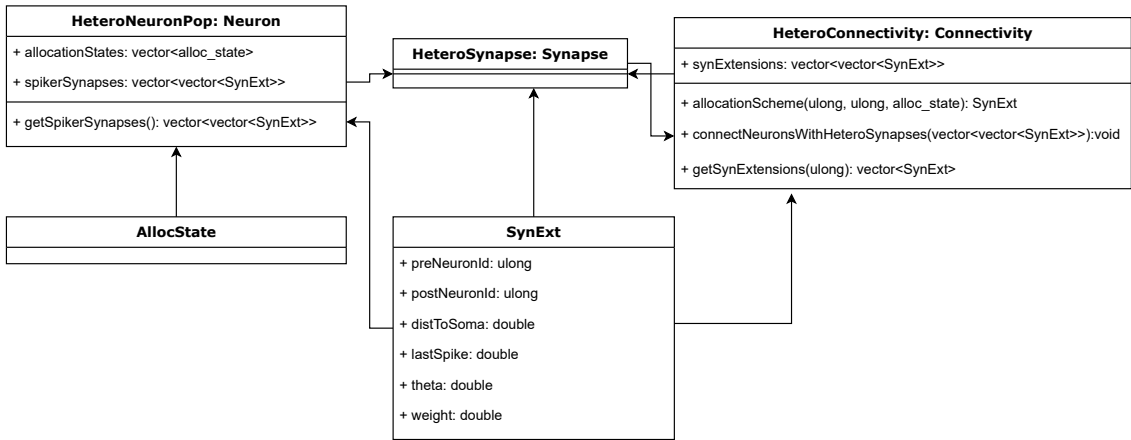


Figure 3.26.: Class diagrams for the HeteroNeuronPop, HeteroSynapse and HeteroConnectivity. Only essential members and methods required for the discussion are included in the figure.

### 3.4.3. Time-stepping scheme

All ODEs in the model, the LIF equation, the cooperativity/ $\theta$  equation, and the synaptic efficacy equation, are updated using the forward Euler time-stepping scheme. The minimum time-step used in the simulations is 0.0001 seconds which is an order of magnitude smaller than the smallest parameter in the model,  $\tau_{delay} = 0.001$  in 3.1.

### 3.4.4. Procedures for extensions

In this section we provide a brief discussion of how the implementation can be extended to change properties of the simulations.

### *3. Pair-based STDP with Heterosynaptic Cooperativity*

---

#### Different dendritic geometries

In the simulations described in previous sections, we use a simplified case of a neuron having a single dendrite with evenly spaced synapses. In order to experiment with different dendritic geometries one could take the following steps:

- Extend the struct AllocationState to include information necessary to make decisions for allocation of new synapses based on one, many or all previous synaptic allocations.
- Extends HeteroConnectivity, overriding the **allocationScheme** method to implement the new synapse allocation strategy.

#### Different cooperativity schemes

Another example for an extension would be the implementation of a new cooperativity rule. For this case, the following step could be used:

- Extend HeteroSynapse, overriding the private method **updateCooperativity** method. This method is called during each advect step of an instance of HeteroSynapse.

#### Different plasticity rules

In order to implement a different plasticity rule, the following step could be used:

- Extend HeteroSynapse, overriding the private method **advectSynapses** method. This method is called during each advect step of an instance of HeteroSynapse.

## **Part III.**

# **Discussion, Limitations and Outlook**



# 4. Discussion, Limitations and Outlook

## 4.1. Discussion

In comparison to other models of heterosynaptic plasticity such as the ones presented in 2.3.1, our model for heterosynaptic cooperativity incorporates fine-grained synaptic communication. Such information sharing equates to dynamic, synaptic coupling that potentially has a significant impact on the dynamics of a network of neurons. In terms of artificial neural networks, heterosynaptic cooperativity may represent some form of regularization that allows the network to obtain robust input configurations when exposed to stimuli. For example, the form of heterosynaptic cooperation presented in this study has a tendency to keep synapses, which would otherwise be silenced by a particular stimulus, to remain moderately active. This phenomenon could translate into the postsynaptic neuron incorporating previously ignored synaptic information. Further evidence is required to determine the consequences of such normalization and, particularly, what may be the benefits of a covariance-based embedding –i.e., one based on activity similarity across inputs– in a supervised problem.

Since our heterosynaptic rule acts to enhance LTP and suppress LTD, it strongly shifts the balance of STDP rules towards potentiation. Such a cooperativity mechanism does not conform to the homeostatic functionality of heterosynaptic rules introduced in section 2.3 for simulation setups described in previous chapters as well as the ones in [5, 15]. In 3.2 we presented the results concerning LTP-drifts in pair-based STDP models with and without heterosynaptic cooperativity. The results provide a clear picture of the effect of cooperation on the runaway dynamics of synapses. In contrast to the heterosynaptic plasticity models in 2.3, cooperativity does not work as a mechanism for homeostasis against runaway dynamics of synapses. This could be an indication that neurons that cooperate in this manner simultaneously incorporate other forms of heterosynaptic plasticity in order to maintain homeostasis.

In section 3.3, we investigated the spatially observable effects of our heterosynaptic cooperation model. Apart from the initial setup, we tuned the baseline LTP parameter,  $B_{LTP}$ , in order to obtain a clear picture of cooperation. We observe that in cases where the kernels for LTP and LTD are similar (high values of  $B_{LTP}$ ), spatial heterosynaptic effects are not prominent and the evolution of the synaptic efficacies are dominated by homosynaptic STDP effects. Nonetheless, the extreme setups of the simulations (large LTD bias or low  $B_{LTP}$ ), allow us to observe how the synapses influence each other. Clearly, in LTD-

#### 4. Discussion, Limitations and Outlook

---

dominant setups, the synapses from median bands that are spatially closer to maximal bands tend to depress slower than median synapses that are more distant to the maximal bands. For large values of  $B_{LTP}$ , the simulations we presented are LTP-dominant and a possibility for the lack of spatially observable patterns in the weight evolution may be accounted for by the possibility that in such strongly LTP biased setups, the median synapses experience rapid LTP in the early parts of the simulation. The dependence of cooperativity on synaptic weights means that synapses then experience increased cooperation, causing the local  $\theta$  term to saturate. The resulting kernels in each synapse would then be a homogeneous, LTP-skewed, STDP kernel.

A particular takeaway from the results is that it is likely that certain parameter sets of the model which preserve more symmetric features of the plasticity kernels and provide stability in terms of the mean synaptic weight, could potentially give rise to observable heterosynaptic patterns as well. As described in [2], stability constitutes the tendency of the mean of the synaptic weights to stabilize around a stable point in between the extremes,  $w_{max}$  and  $w_{min}$ . In lieu of this possibility, we analyzed synaptic stability of a single neuron with heterosynaptic STDP using the framework in [2]. However, since we were unable to reproduce the results for the non-heterosynaptic case, we did not proceed further in this direction. However, a brief discussion regarding the topic is presented in the section A.4.

In reference to the role of heterosynaptic plasticity as a facilitator for synaptic competition (introduced in section 2.3), at this point our simulations and results do not allow us to make an objectively explicit statement regarding the coherence of such a role with the heterosynaptic cooperativity model we have devised. Nonetheless, since our rule enforces cooperativity more prominently when a pair of synapses are both strongly potentiated, a reasonable expectation would be that they cooperate to reinforce their respective strengths whereas weak pairs refrain from cooperation. Once more, simulations setups in [2] could provide a framework for investigating such a hypothesis.

## 4.2. Assumptions and Limitations

It is important to note the limitations of our heterosynaptic cooperativity model and its implications. As mentioned in the introduction of the model, we derive the dynamics of  $\theta$  from an experimental study published in 2020 [28]. Recalling the results from the paper, it essentially presents the following data:

- Single spine LTP induction with pre-post timings of +7 ms and +13 ms.
- Double spine LTP induction with pre-post timings of +7 ms and +13 ms for multiple interspine distances.
- Single spine LTD induction with post-pre timings of -15 ms and -23 ms.

- Double spine LTD induction with post-pre timings of -15 ms and -23 ms for multiple interspine distances.

Due to the limited number of data points, the model we derived is characterized by multiple assumptions which may or may not correctly capture the phenomenon we observe on a broader scope. Each of the assumptions can be interpreted as a limitation since we cannot present evidence supporting them. The following are some of the assumptions that were made in order to define a complete model:

- Heterosynaptic cooperativity between two coincidentally stimulated synapses decays exponentially with increasing distance between them. More experimental data would be required to confirm such a relationship.
- Heterosynaptic cooperativity decays exponentially with increasing difference in timing of presynaptic inputs on coincidentally stimulated synapses. More experimental data would be required to confirm such a relationship.
- Cooperativity between synapses is a function of the product of the efficacies of the two synapses.
- Cooperativity is an additive, local property of synapses, meaning that a coincident three-synapse induction is treated as three dependent two-synapse inductions. It is reasonable to categorize this as a major simplification as it is likely that as more synapses are stimulated together they compete for the extracellular calcium, which is limited.
- The relative effect of cooperativity on the STDP kernel decreases as the magnitude of the cooperativity increases.

In our work, we loosely associate the cooperativity variable,  $\theta$ , as a tracker for intracellular calcium due to synaptic cooperation. However, at this point, we are unable to verify the degree of validity of such an association. Information in this regard would have implications on the decay constant of  $\theta$  as well as the window for the coincidence of presynaptic inputs. Additionally, the model does not account for a potential scarcity of extracellular calcium after a series of cooperativity spikes, ignoring resource limitations which are likely.

Finally, it is clear that the dynamics of cooperativity are defined by multiple parameters. This increases both the analytic and numerical complexity of the model, making it more difficult to analyse and obtain a complete overview of the system.

## 4.3. Outlook

In the previous chapters, we introduced our model for heterosynaptic cooperativity and analyzed the spatial effects that arise from it. Nonetheless, the model includes numerous parameters and the effect of these parameters on the behavior of the synapses would

#### *4. Discussion, Limitations and Outlook*

---

require further investigation and analysis. In this section, we discuss ideas for further analysis of our model.

An important step towards fully understanding the implications of our heterosynaptic rule is to obtain analytical expressions that elicit information regarding the sensitivity of the plasticity of synapses as well as the firing rate of the postsynaptic neuron to different parameters in the model. This process would be supplemented by simulations or tests designed to demonstrate the expected behavior. This would allow us to gain insight on scaling requirements for cooperativity based on the number of synapses on a dendritic tree, the average gap between synapses, the spatial and temporal decay parameters of the cooperativity, etc., in order to control the postsynaptic firing rate.

Additionally, from the perspective of dynamics of a single neuron, interesting insights can be obtained by doing stability and competition analysis of pair-based STDP supplemented with heterosynaptic cooperativity. Such analysis can provide an understanding of the type of weight normalization that heterosynaptic STDP models may require in order to reach steady-state weight distributions as well as the range of parameter sets that can induce Hebbian-type synaptic competition. A similar analysis was already been published on purely homosynaptic STDP models including pair-based models, triplet, quadruplet, and NMDAR-based models [2].

Once an elaborate understanding of single neuron dynamics due to heterosynaptic cooperativity is obtained, the experiments can be extended to one or more populations of neurons. Such experiments can shed light on how different cooperativity rules affect the activity patterns of different groups of neurons in the population. This can, in turn, allow an elaborate comparative study between network simulations that allow cooperativity and those that are purely homosynaptic.

# **Appendix**



# A. Appendix

## A.1. Synaptic weight normalization

In our simulations we require our synapses to always maintain their weights between  $w_{min}$  (=0) and  $w_{max}$  (=2). Under STDP, such a range would not be maintained unless the synapses are limited in some manner [2]. In our simulations we impose a hard bounds on the synapses such that each time a synapse undergoes a plastic change, it is thereafter passed through the following function:

$$w_i = \max(w_{min}, \min(w_i, w_{max})) \quad (\text{A.1})$$

Other forms of imposing such bounds exist but in order to preserve simplicity we use the one above.

## A.2. Additional results for LTP drift in pair-based STDP

In this section, we present the results of our LTP drift simulations that are not presented in the main discussion.

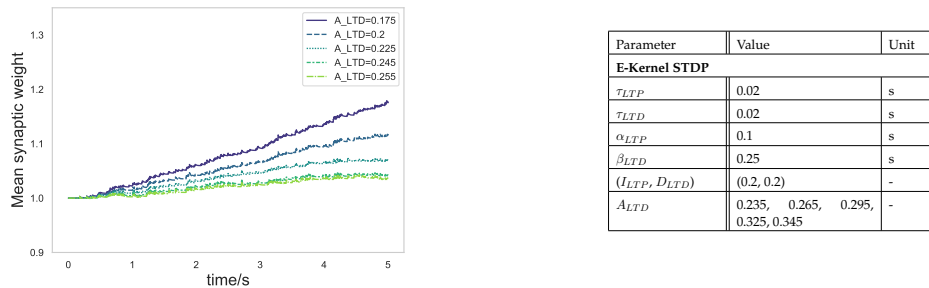
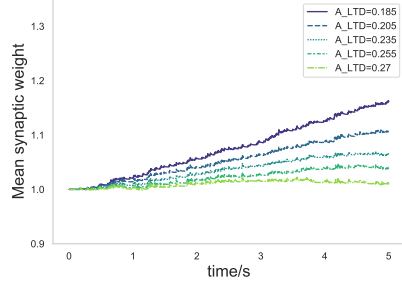


Figure A.1.: **Left:** LTP drift for E-Kernel heterosynaptic cooperativity,  $\alpha_{LTP} = 0.1$ ,  $\beta_{LTD} = 0.25$ .  
**Right:** Parameters specific to the set of simulations.

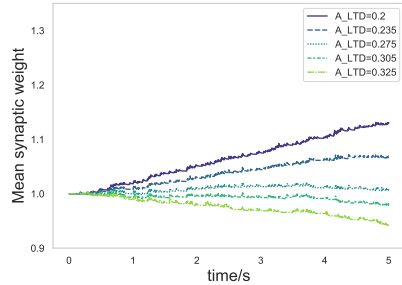
## A. Appendix

---



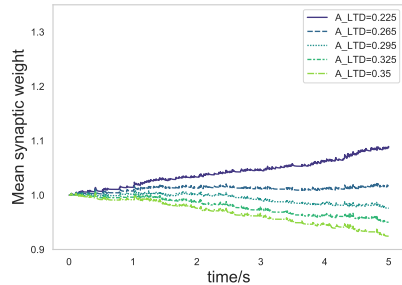
Parameter	Value	Unit
<b>E-Kernel STDP</b>		
$\tau_{LTP}$	0.02	s
$\tau_{LTD}$	0.02	s
$\alpha_{LTP}$	0.1	s
$\beta_{LTD}$	0.25	s
$(I_{LTP}, D_{LTD})$	(1.0, 1.0)	-
$A_{LTD}$	0.235, 0.265, 0.295, 0.325, 0.345	-

Figure A.2.: **Left:** LTP drift for E-Kernel heterosynaptic cooperativity,  $\alpha_{LTP} = 0.1$ ,  $\beta_{LTD} = 0.25$ .  
**Right:** Parameters specific to the set of simulations.



Parameter	Value	Unit
<b>E-Kernel STDP</b>		
$\tau_{LTP}$	0.02	s
$\tau_{LTD}$	0.02	s
$\alpha_{LTP}$	0.1	s
$\beta_{LTD}$	0.25	s
$(I_{LTP}, D_{LTD})$	(1.0, 1.0)	-
$A_{LTD}$	0.235, 0.265, 0.295, 0.325, 0.345	-

Figure A.3.: **Left:** LTP drift for E-Kernel heterosynaptic cooperativity,  $\alpha_{LTP} = 0.1$ ,  $\beta_{LTD} = 0.25$ .  
**Right:** Parameters specific to the set of simulations.



Parameter	Value	Unit
<b>E-Kernel STDP</b>		
$\tau_{LTP}$	0.02	s
$\tau_{LTD}$	0.02	s
$\alpha_{LTP}$	0.1	s
$\beta_{LTD}$	0.25	s
$(I_{LTP}, D_{LTD})$	(1.0, 1.0)	-
$A_{LTD}$	0.235, 0.265, 0.295, 0.325, 0.345	-

Figure A.4.: **Left:** LTP drift for E-Kernel heterosynaptic cooperativity,  $\alpha_{LTP} = 0.1$ ,  $\beta_{LTD} = 0.25$ .  
**Right:** Parameters specific to the set of simulations.

## A.2. Additional results for LTP drift in pair-based STDP

---

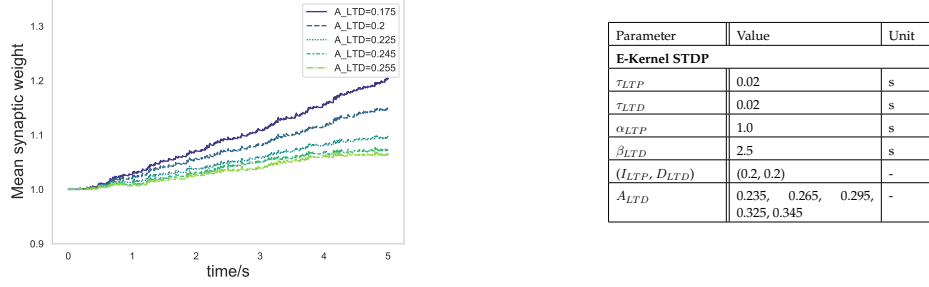


Figure A.5.: **Left:** LTP drift for E-Kernel heterosynaptic cooperativity,  $\alpha_{LTP} = 1.0$ ,  $\beta_{LTD} = 2.5$ .  
**Right:** Parameters specific to the set of simulations.

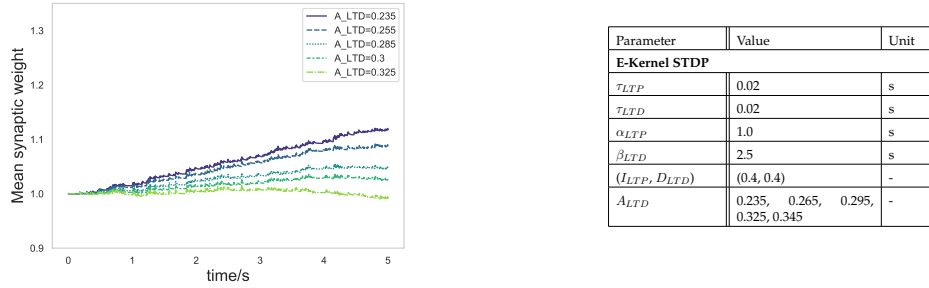


Figure A.6.: **Left:** LTP drift for E-Kernel heterosynaptic cooperativity,  $\alpha_{LTP} = 1.0$ ,  $\beta_{LTD} = 2.5$ .  
**Right:** Parameters specific to the set of simulations.

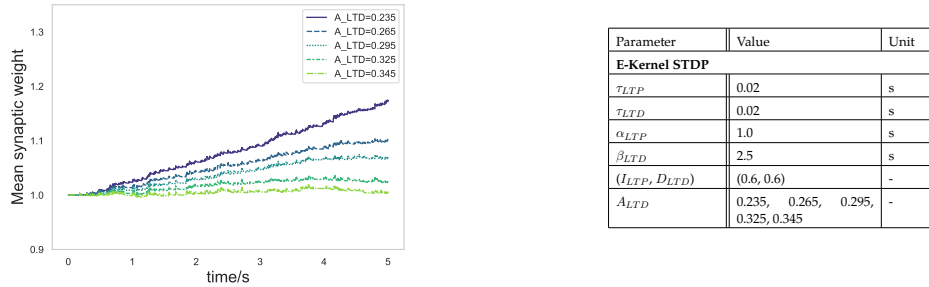
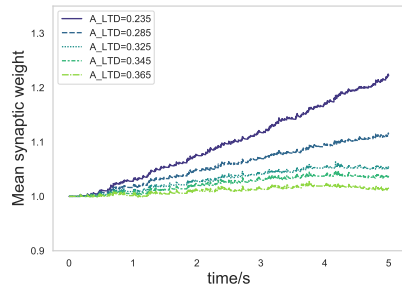


Figure A.7.: **Left:** LTP drift for E-Kernel heterosynaptic cooperativity,  $\alpha_{LTP} = 1.0$ ,  $\beta_{LTD} = 2.5$ .  
**Right:** Parameters specific to the set of simulations.

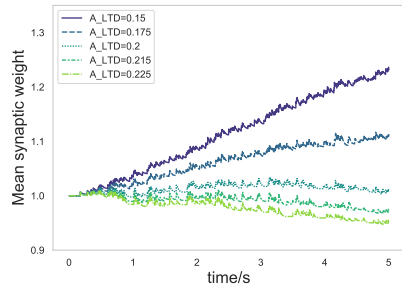
## A. Appendix

---



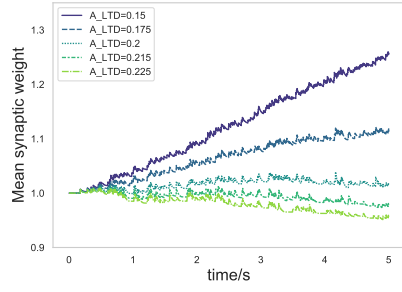
Parameter	Value	Unit
<b>E-Kernel STDP</b>		
$\tau_{LTP}$	0.02	s
$\tau_{LTD}$	0.02	s
$\alpha_{LTP}$	1.0	s
$\beta_{LTD}$	2.5	s
$(I_{LTP}, D_{LTD})$	(0.8, 0.8)	-
$A_{LTD}$	0.235, 0.265, 0.295, 0.325, 0.345	-

Figure A.8.: **Left:** LTP drift for E-Kernel heterosynaptic cooperativity,  $\alpha_{LTP} = 1.0$ ,  $\beta_{LTD} = 2.5$ .  
**Right:** Parameters specific to the set of simulations.



Parameter	Value	Unit
<b>E-Kernel STDP</b>		
$\tau_{LTP}$	0.02	s
$\tau_{LTD}$	0.02	s
$\alpha_{LTP}$	0.1	s
$\beta_{LTD}$	0.25	s
$(I_{LTP}, D_{LTD})$	(0.2, 0.2)	-
$A_{LTD}$	0.235, 0.265, 0.295, 0.325, 0.345	-

Figure A.9.: **Left:** LTP drift for G-Kernel heterosynaptic cooperativity,  $\alpha_{LTP} = 0.1$ ,  $\beta_{LTD} = 0.25$ .  
**Right:** Parameters specific to the set of simulations.



Parameter	Value	Unit
<b>E-Kernel STDP</b>		
$\tau_{LTP}$	0.02	s
$\tau_{LTD}$	0.02	s
$\alpha_{LTP}$	0.1	s
$\beta_{LTD}$	0.25	s
$(I_{LTP}, D_{LTD})$	(0.4, 0.4)	-
$A_{LTD}$	0.235, 0.265, 0.295, 0.325, 0.345	-

Figure A.10.: **Left:** LTP drift for G-Kernel heterosynaptic cooperativity,  $\alpha_{LTP} = 0.1$ ,  $\beta_{LTD} = 0.25$ .  
**Right:** Parameters specific to the set of simulations.

## A.2. Additional results for LTP drift in pair-based STDP

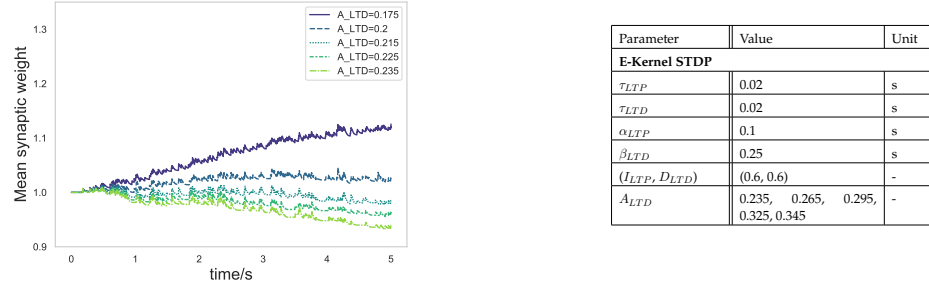


Figure A.11.: **Left:** LTP drift for G-Kernel heterosynaptic cooperativity,  $\alpha_{LTP} = 0.1$ ,  $\beta_{LTD} = 0.25$ .  
**Right:** Parameters specific to the set of simulations.

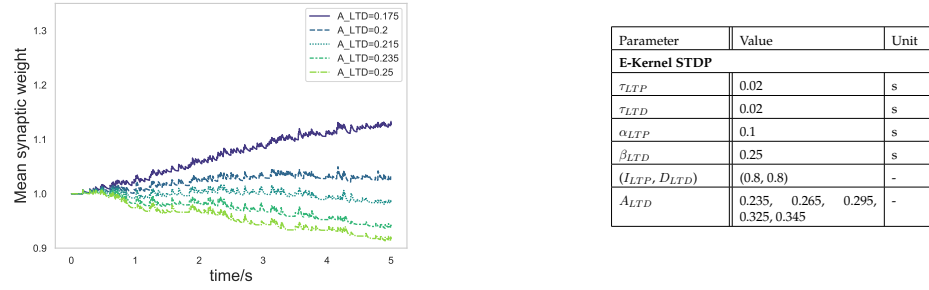


Figure A.12.: **Left:** LTP drift for G-Kernel heterosynaptic cooperativity,  $\alpha_{LTP} = 0.1$ ,  $\beta_{LTD} = 0.25$ .  
**Right:** Parameters specific to the set of simulations.

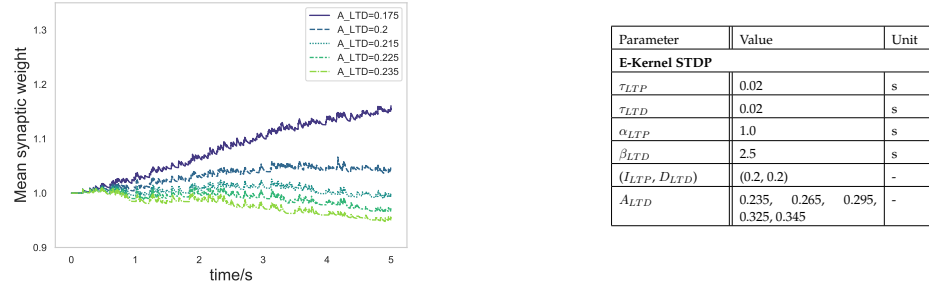
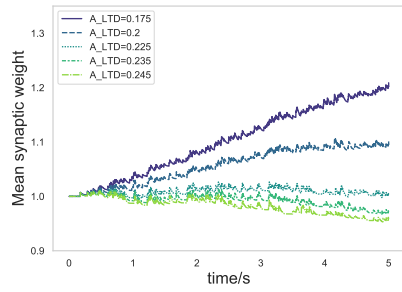


Figure A.13.: **Left:** LTP drift for G-Kernel heterosynaptic cooperativity,  $\alpha_{LTP} = 1.0$ ,  $\beta_{LTD} = 2.5$ .  
**Right:** Parameters specific to the set of simulations.

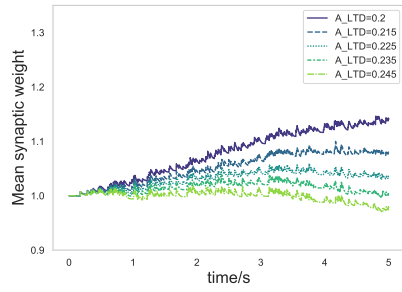
## A. Appendix

---



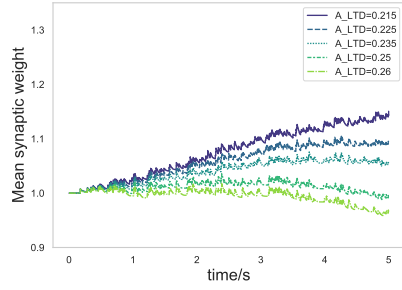
Parameter	Value	Unit
<b>E-Kernel STDP</b>		
$\tau_{LTP}$	0.02	s
$\tau_{LTD}$	0.02	s
$\alpha_{LTP}$	1.0	s
$\beta_{LTD}$	2.5	s
$(I_{LTP}, D_{LTD})$	(0.4, 0.4)	-
$A_{LTD}$	0.235, 0.265, 0.295, 0.325, 0.345	-

Figure A.14.: **Left:** LTP drift for G-Kernel heterosynaptic cooperativity,  $\alpha_{LTP} = 1.0$ ,  $\beta_{LTD} = 2.5$ .  
**Right:** Parameters specific to the set of simulations.



Parameter	Value	Unit
<b>E-Kernel STDP</b>		
$\tau_{LTP}$	0.02	s
$\tau_{LTD}$	0.02	s
$\alpha_{LTP}$	1.0	s
$\beta_{LTD}$	2.5	s
$(I_{LTP}, D_{LTD})$	(0.6, 0.6)	-
$A_{LTD}$	0.235, 0.265, 0.295, 0.325, 0.345	-

Figure A.15.: **Left:** LTP drift for G-Kernel heterosynaptic cooperativity,  $\alpha_{LTP} = 1.0$ ,  $\beta_{LTD} = 2.5$ .  
**Right:** Parameters specific to the set of simulations.



Parameter	Value	Unit
<b>E-Kernel STDP</b>		
$\tau_{LTP}$	0.02	s
$\tau_{LTD}$	0.02	s
$\alpha_{LTP}$	1.0	s
$\beta_{LTD}$	2.5	s
$(I_{LTP}, D_{LTD})$	(0.8, 0.8)	-
$A_{LTD}$	0.235, 0.265, 0.295, 0.325, 0.345	-

Figure A.16.: **Left:** LTP drift for G-Kernel heterosynaptic cooperativity,  $\alpha_{LTP} = 1.0$ ,  $\beta_{LTD} = 2.5$ .  
**Right:** Parameters specific to the set of simulations.

### A.3. Additional simulation results for spatial effect

In this section, we present the results of our spatial simulations that are not presented in the main discussion.

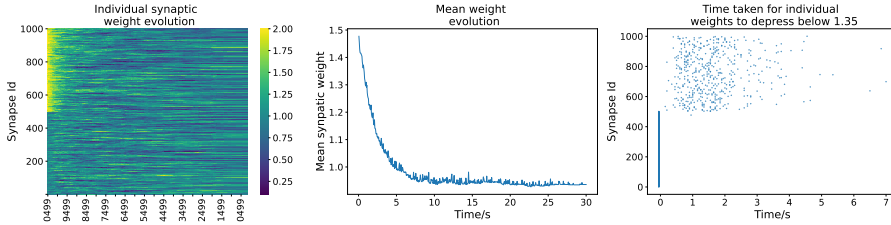


Figure A.17.: E-Kernel simulation with no heterosynaptic cooperativity,  $B_{LTP} = 1.0$ . The figures present data averaged over 10 runs with different seeds. **Left:** Figure shows the evolution of individual synaptic weights over the course of the simulation. **Middle:** Figure shows the evolution of the mean synaptic weight. The scenario is LTD dominant and the mean of the weights stabilises below 1. **Right:** Figure shows the time take by each of the synapse weights to drop below 1.35.

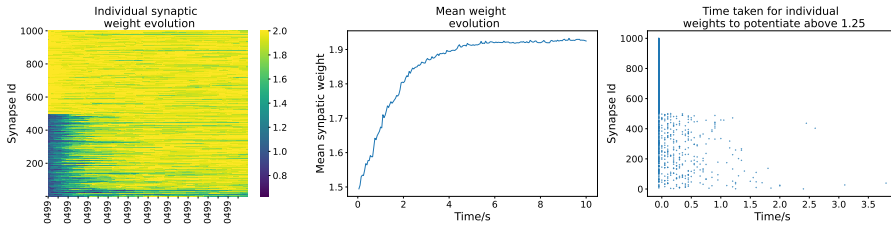


Figure A.18.: E-Kernel simulation with heterosynaptic cooperativity,  $B_{LTP} = 1.0$ . The figures present data averaged over 10 runs with different seeds. **Left:** Figure shows the evolution of individual synaptic weights over the course of the simulation. **Middle:** Figure shows the evolution of the mean synaptic weight. The scenario is LTP dominant and the mean of the weights stabilises around 1.9. **Right:** Figure shows the time take by each of the synapse weights to potentiate above 1.25.

## A. Appendix

---

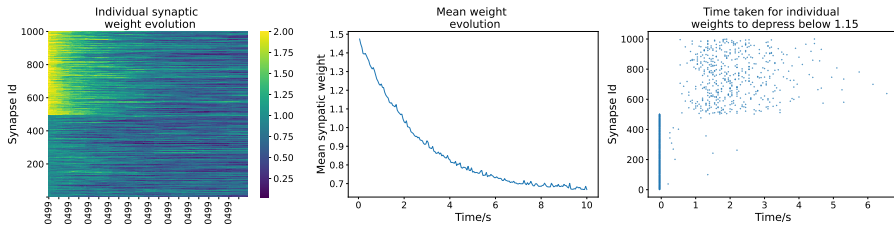


Figure A.19.: E-Kernel simulation with no heterosynaptic cooperativity,  $B_{LTP} = 0.75$ . The figures present data averaged over 10 runs with different seeds. **Left:** Figure shows the evolution of individual synaptic weights over the course of the simulation. **Middle:** Figure shows the evolution of the mean synaptic weight. The scenario is LTD dominant and the mean of the weights stabilises around 0.7. **Right:** Figure shows the time take by each of the synapse weights to drop below 1.15.

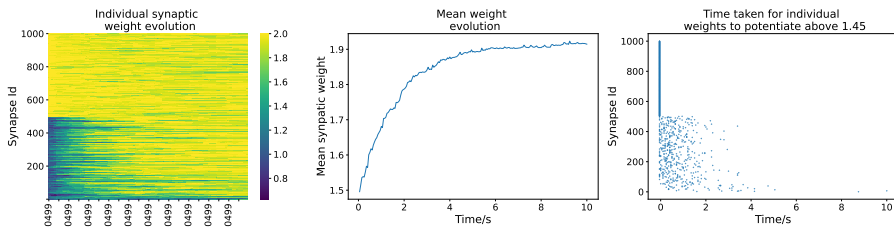


Figure A.20.: E-Kernel simulation with heterosynaptic cooperativity,  $B_{LTP} = 0.75$ . The figures present data averaged over 10 runs with different seeds. **Left:** Figure shows the evolution of individual synaptic weights over the course of the simulation. **Middle:** Figure shows the evolution of the mean synaptic weight. The scenario is LTP dominant and the mean of the weights stabilises around 2. **Right:** Figure shows the time take by each of the synapse weights to potentiate above 1.45.

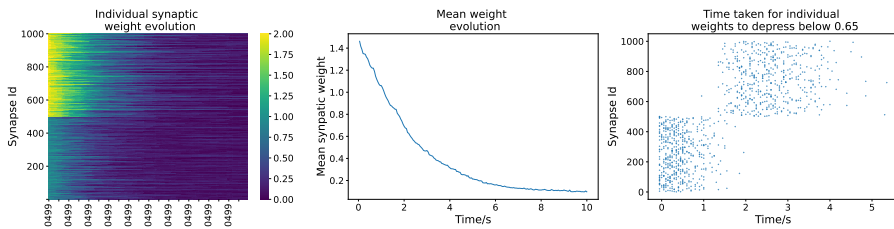


Figure A.21.: E-Kernel simulation with no heterosynaptic cooperativity,  $B_{LTP} = 0.25$ . The figures present data averaged over 10 runs with different seeds. **Left:** Figure shows the evolution of individual synaptic weights over the course of the simulation. **Middle:** Figure shows the evolution of the mean synaptic weight. The scenario is LTD dominant and the mean of the weights stabilises around 0.2. **Right:** Figure shows the time take by each of the synapse weights to drop below 0.65.

### A.3. Additional simulation results for spatial effect

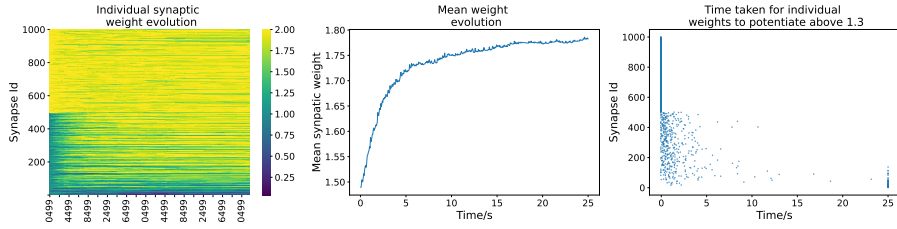


Figure A.22.: E-Kernel simulation with heterosynaptic cooperativity,  $B_{LTP} = 0.25$ . The figures present data averaged over 10 runs with different seeds. **Left:** Figure shows the evolution of individual synaptic weights over the course of the simulation. **Middle:** Figure shows the evolution of the mean synaptic weight. The scenario is LTP dominant and the mean of the weights stabilises around 2.0. **Right:** Figure shows the time take by each of the synapse weights to potentiate above 1.8.

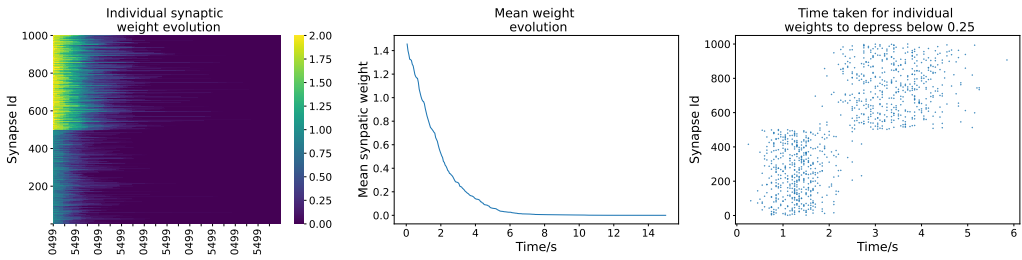


Figure A.23.: E-Kernel simulation with no heterosynaptic cooperativity,  $B_{LTP} = 0.0$ . The figures present data averaged over 10 runs with different seeds. **Left:** Figure shows the evolution of individual synaptic weights over the course of the simulation. **Middle:** Figure shows the evolution of the mean synaptic weight. The scenario is LTD dominant and the mean of the weights stabilises around 0. **Right:** Figure shows the time take by each of the synapse weights to drop below 0.25.

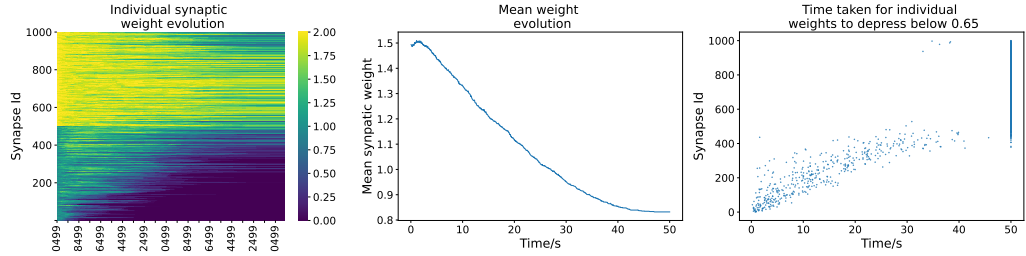


Figure A.24.: E-Kernel simulation with heterosynaptic cooperativity,  $B_{LTP} = 0.0$ . The figures present data averaged over 10 runs with different seeds. **Left:** Figure shows the evolution of individual synaptic weights over the course of the simulation. **Middle:** Figure shows the evolution of the mean synaptic weight. The scenario is LTD dominant and the mean of the weights stabilises around 0.8. **Right:** Figure shows the time take by each of the synapse weights to drop below 0.65.

## A.4. Single neuron synaptic stability

In the process of analyzing the heterosynaptic cooperativity model, we investigated the synaptic stability of a single neuron according to the simulation setup in [2].

In [2], a plasticity rule can be categorized as stable, partially stable, and unstable. An STDP model is considered unconditionally stable if the individual synaptic weights never exceed the bounds of the weight range ( $w_{min}$ - $w_{max}$ ) without the need for explicit bounds on the weights and the mean weight of the synapses stabilize at a fixed point. On the other hand, in partially stable models, the mean synaptic weight stabilizes at a fixed point within the bounds of the weight range only when there exist explicit bounds for the individual weights. Finally, a model is said to be unstable when the synaptic weights converge to either of the boundaries of the weight range in case of explicit bounding, otherwise, they exceed the bounds and potentiate/depress indefinitely.

We attempted to replicate the non-heterosynaptic, pair-based STDP results presented in [2]. We were able to obtain a stable point around which the mean synaptic weight fluctuates. We further analyzed the distribution of the weights of the synapses at the end of the simulation. However, we were unable to reproduce the U-shaped distribution of synaptic weights at the end of the simulation. This could potentially be due to the large values of  $ALTP$  and  $ALTD$  used in our simulations. However, given the large number of parameters, the discrepancy could potentially be a multi-parameter effect which we were unable to fully uncover.





# Bibliography

- [1] Citri A. and Malenka RC. Synaptic plasticity: multiple forms functions, and mechanisms., 2007.
- [2] Babadi B. and Abbott LF. Stability and competition in multi-spike models of spike-timing dependent plasticity. PLOS Computational Biolog, 2016.
- [3] Henry Buchtel. Neuronal plasticity: Historical roots and evolution of meaning. Experimental Brain Research., 2008.
- [4] Bell C. C., Han V. Z., Sugawara Y., , and Grant K. Synaptic plasticity in a cerebellum-like structure depends on temporal order. Nature 387, 1997.
- [5] Marina Chistiakova, Nicholas M. Bannon, Maxim Bazhenov, and Maxim Volgushev. Heterosynaptic plasticity: Multiple mechanisms and multiple roles. Neuroscientist, 2014.
- [6] Schuman EM and Madison DV. Locally distributed synaptic potentiation in the hippocampus. Science, 1994.
- [7] Engert F. and Bonhoeffer. Synapse specificity of long-term potentiation breaks down at short distances. Nature 3308, 1997.
- [8] Daniel E. Feldman. Neural circuit and cognitive development (second edition)., 2020.
- [9] Wulfram Gerstner, Werner M. Kistler, Richard Naud, and Liam Paninski. Neuronal dynamics: From single neurons to networks and models of cognition. Cambridge University Press, 2014.
- [10] Michael Graupner and Nicolas Brunel. Calcium-based plasticity model explains sensitivity of synaptic changes to spike pattern, rate, and dendritic location., 2012.
- [11] Lynch GS., Dunwiddie T., and Gribkoff V. Heterosynaptic depression: a postsynaptic correlate of long-term potentiation. Nature 266:737–9, 1977.
- [12] Lodish H., Berk A., Zipursky SL., and et al. Overview of neuron structure and function. <https://www.ncbi.nlm.nih.gov/books/NBK21535>, 2000.
- [13] Markram H., Lübke J., Frotscher M., and Sakmann B. Regulation of synaptic efficacy by coincidence of postsynaptic ap and epsp. Science 275, 1997.

## Bibliography

---

- [14] D.O. Hebb. The organization of behavior; a neuropsychological theory. Wiley, 1949.
- [15] Chen JY, Lonjers P., Lee C., Chistiakova M., Volgushev M., and Bazhenov M. Heterosynaptic plasticity prevents runaway synaptic dynamics. *J Neurosci.*, 2013.
- [16] Christopher M Lee, Carl Stoelzel, Marina Chistiakova, and Maxim Volgushev. Heterosynaptic plasticity induced by intracellular tetanization in layer 2/3 pyramidal neurons in rat auditory cortex., 2012.
- [17] Volgushev M., Voronin LL., Chistiakova M., and Singer W. Induction of ltp and ltd in visual cortex neurones by intracellular tetanization., 1994.
- [18] Chistiakova Marina and Maxim Volgushev. Heterosynaptic plasticity in the neocortex. *Experimental brain research* vol. 199,3-4, 2009.
- [19] Thomas Nevian and Bert Sakmann. Spine ca2 signaling in spike-timing-dependent plasticity., 2006.
- [20] Roger A. Nicoll. A brief history of long-term potentiation. *Neuron.*, 2016.
- [21] Bliss T. V. P., , and Gardner-Medwin A. R. Long-lasting potentiation of synaptic transmission in the dentate area of the unanaesthetized rabbit following stimulation of the perforant path. *J. Physiol.* 232, 1973.
- [22] Bliss T. V. P., , and Lømo T. Long-lasting potentiation of synaptic transmission in the dentate area of the anaesthetized rabbit following stimulation of the perforant path. *J. Physiol.* 232, 1973.
- [23] Dayan Peter and L. F. Abbott. Theoretical neuroscience: Computational and mathematical modeling of neural systems., 2005.
- [24] Jean-Pascal Pfister and Wulfram Gerstner. Triplets of spikes in a model of spike timing-dependent plasticity. *Journal of Neuroscience*, 2006.
- [25] Kandel E. R., Schwartz J. H., and Jessell T. M. Principles of neural science. McGraw-Hill, Health Professions Division., 2000.
- [26] Malenka RC. and Bear MF. Ltp and ltd: an embarrassment of riches. *Neuron*, 2004.
- [27] Royer S. and Paré D. Conservation of total synaptic weight through balanced synaptic depression and potentiation. *Nature* 422, 2003.
- [28] Tazerart S., Mitchell D.E., Miranda-Rottmann S., and et al. A spike-timing-dependent plasticity rule for dendritic spines. *Nat Commun* 11, 4276, 2020.
- [29] Harel Z. Shouval, Samuel S.H. Wang, and Gayle M. Wittenberg. Spike timing dependent plasticity: a consequence of more fundamental learning rules. *Frontier Computational Neuroscience*, 2010.

---

*Bibliography*

- [30] Per Jesper Sjöström, Gina G. Turrigiano, and Sacha B Nelson. Rate, timing, and cooperativity jointly determine cortical synaptic plasticity. *Neuron*, 2001.
- [31] Bonhoeffer T., Staiger V., and Aersten A. Synaptic plasticity in rat hippocampal slice cultures: local “hebbian” conjunction of pre- and postsynaptic stimulation leads to distributed synaptic enhancement. *PNAS*, 1989.
- [32] Dunwiddie T. and Lynch G. Long-term potentiation and depression of synaptic responses in the rat hippocampus: localization and frequency dependency. *J Physiol.*, 1978.
- [33] Kuhnt U. and Voronin LL. Interaction between paired-pulse facilitation and long-term potentiation in area ca1 of guinea-pig hippocampal slices: application of quantal analysis. *Neuroscience*, 1994.
- [34] Huai-Xing Wang, Richard C Gerkin, David W Nauen, and Guo-Qiang Bi. Coactivation and timing-dependent integration of synaptic potentiation and depression, 2005.
- [35] Gayle M. Wittenberg and Samuel S.-H. Wang. Malleability of spike-timing-dependent plasticity at the ca3–ca1 synapse. *Journal of Neuroscience* 26 (24) 6610-6617, 2006.
- [36] Li X., Luo S., and Xue F. Effects of synaptic integration on the dynamics and computational performance of spiking neural network. *Cogn Neurodyn.g*, 2020.